



**University of
Zurich^{UZH}**

Department of Geography

Environmental stress impacts on plant functioning: Insights from common and new Earth observation approaches

Master Thesis – GEO 511

April 20th, 2017

Tiziana Speckert

09-729-807

Supervision by: PD Dr. Alexander Damm

Member of Faculty: Prof. Dr. Michael E. Schaepman

Abstract

Sun-induced chlorophyll fluorescence (SIF) is a new Earth observation approach which can be directly related to photosynthetic efficiency of plants. SIF is a small signal in the radiance spectrum and can be detected passively with remote sensing spectrometers. In this master thesis, SIF was retrieved in two oxygen absorption bands at 680nm (SIF₆₈₀) and 760nm (SIF₇₆₀) with the improved Fraunhofer Line Discrimination (iFLD) module. Both SIF signals were simultaneously acquired and applied to monitor plant functioning under environmental stress impacts. Field experiments with light, heat and water as abiotic stressors were conducted with different plants (corn, barley, rapeseed, sugar beet and wheat) and at different time scales. The measured SIF was compared with common vegetation indices (VIs) to analyse plant stress responses and underlying processes. Both SIF and VIs were statistically analysed and illustrated in maps. In addition, fluorescence stress indices were evaluated and the three experiments were located in a bi-dimensional parameter space. The calculation of the stress intensity fluorescence index (SIFI) displayed high capability in stress recognition. Moreover, the outcomes demonstrated the benefit of SIF to detect actual plant stress responses and provided potential insights into plant functioning. Compared with the VIs, SIF observes plant stress responses more quickly and unfolds high added value.

Declaration

I hereby declare that the submitted thesis is the result of my own, independent work. All external sources are explicitly acknowledged in the thesis.

Tiziana Speckert

Acknowledgements

First of all I would like to thank my supervisor PD Dr. Alexander Damm for his willingness to support this master thesis and helpful advice. The door to his office was always open whenever I had a question. I am extremely thankful to him for his confidence and efforts.

I am also grateful to my family and friends for their support and sympathy. I especially would like to thank my parents, who enabled me to study and supported me all the years.

Abbreviations

ABA	Absciscic acid
ATP	Adenosine triphosphate
A₀	Primary acceptor molecule
A₁	Phylloquinone
CET	Cyclic electron transport
ESA	European Space Agency
EVI	Enhanced vegetation index
Fd	Ferredoxin
FLEX	Fluorescence Explorer
FLD	Fraunhofer Line Discrimination
3FLD	modified Fraunhofer Line Discrimination
iFLD	improved Fraunhofer Line Discrimination
GPP	Gross primary production
HSPs	Heat shock proteins
HyPlant	Hyperspectral Plant Imaging Spectrometer
LAI	Leaf area index
LET	Linear electron transport
MSI	Moisture stress index
NADP	Nicotinamide adenine dinucleotide phosphate
NDII	Normalized difference infra-red index
NDNI	Normalized difference nitrogen index
NDVI	Normalized Difference vegetation index
NDWI	Normalized difference water index
NPQ	Non-photochemical quenching

OEC	Oxygen evolving complex
PAR	Photosynthetic active radiation
PRI	Photochemical reflectance index
PSI	Photosystem I
PSII	Photosystem II
P680	Photosynthetic pigments of PSII
P700	Photosynthetic pigments of PSI
Q_a	Quinone a
Q_b	Quinone b
ROI	Region of interest
ROS	Reactive oxygen species
Rubisco	Ribulose-1,5-bisphosphate carboxylase/oxygenase
RuBP	Ribulose-1,2-bisphosphate
SIF	Sun-induced chlorophyll fluorescence
SIF₆₈₀	Sun-induced chlorophyll fluorescence at 680nm
SIF₇₆₀	Sun-induced chlorophyll fluorescence at 760nm
SR	Simple ratio
VI_s	Vegetation Indices
WBI	Water band index

Contents

- Abstract** **i**
- Declaration** **ii**
- Acknowledgements** **iii**
- List of Figures** **viii**
- List of Tables** **ix**
- 1 Introduction** **1**
- 2 Background** **4**
 - 2.1 Photosynthesis 4
 - 2.2 Abiotic plant stress responses 7
 - 2.2.1 Heat stress responses 7
 - 2.2.2 Light stress responses 9
 - 2.2.3 Water stress responses 10
- 3 Methods** **12**
 - 3.1 Study Areas 12
 - 3.2 Experiments 13
 - 3.2.1 Heat stress 13
 - 3.2.2 Light stress 13
 - 3.2.3 Water stress 14
 - 3.3 HyPlant data acquisition and pre-processing 15
 - 3.4 Retrieval of vegetation indices and fluorescence 16
 - 3.4.1 Retrieval of vegetation indices 16
 - 3.4.2 Retrieval of fluorescence 18
 - 3.5 Stress indicators 20
- 4 Results** **23**
 - 4.1 Heat stress 23
 - 4.1.1 Sun-induced chlorophyll fluorescence 23
 - 4.1.2 Vegetation indices 23
 - 4.1.3 Stress Fluorescence Index 27
 - 4.1.4 Pearson correlation between sun-induced chlorophyll fluorescence and vegetation indices 27
 - 4.2 Light stress 28

4.2.1	Sun-induced chlorophyll fluorescence and simple ratio	29
4.2.2	Light Stressed Fluorescence Index	30
4.2.3	Pearson correlation	30
4.3	Water stress	32
4.3.1	Sun-induced chlorophyll fluorescence and simple ratio	32
4.3.2	Water Stress Fluorescence Index	34
4.3.3	Pearson correlation between sun-induced chlorophyll fluorescence and simple ratio	36
4.4	Bi-dimensional parameter space of vegetation stress	36
4.4.1	Heat stress	38
4.4.2	Light stress	38
4.4.3	Water stress	39
5	Discussion	40
5.1	Experimental settings	40
5.2	Reliability of sun-induced chlorophyll fluorescence	40
5.3	Sensitivity of sun-induced chlorophyll fluorescence for environmental stress	41
5.3.1	Heat stress experiment	41
5.3.2	Light stress experiment	42
5.3.3	Water stress experiment	44
5.4	Monitoring of environmental stress impacts	45
6	Conclusion	47
	References	56
	Appendix	57

List of Figures

- Figure 1** PSI and PSII fluorescence 5
- Figure 2** Photosynthetic linear electron transport 6
- Figure 3** Study areas 12
- Figure 4** Experimental set up of the light experiment 14
- Figure 5** Water stressed and unstressed sugar beet 14
- Figure 6** HyPlant sensor 16
- Figure 7** Bi-dimensional parameter space 21
- Figure 8** SIF and VI maps of the heat stress experiment 24
- Figure 9** Boxplots of the heat stress experiment 25
- Figure 10** SIFI and TSFI boxplots and maps 27
- Figure 11** SIF and SR maps of the light stress experiment 29
- Figure 12** Scatterplots of the light stress experiment 30
- Figure 13** SIFI and LSFI of light stressed sugar beet 31
- Figure 14** SIF₆₈₀ maps of sugar beet during the water stress experiment 32
- Figure 15** Boxplots from the water stress experiment 33
- Figure 16** SIFI and WSFI boxplots of the water stress experiment 34
- Figure 17** SIFI and WSFI maps of the water stress experiment 35
- Figure 18** Bi-dimensional parameter space with all experiments 36
- Figure 19** Heat stress representation in the bi-dimensional parameter space 37
- Figure 20** Light stress representation in the bi-dimensional parameter space 38
- Figure 21** Water stress representation in the bi-dimensional parameter space 39
- Figure 22** Kautsky effect 43
- Figure 23** NDII 57

List of Tables

Table 1	Abiotic stress responses	8
Table 2	Acquisition details of each experiment	15
Table 3	Pearson correlation	28

1 Introduction

Ongoing climate change entails global warming and an increased frequency of extreme climate and weather events. In addition, it involves changes in precipitation and atmospheric composition. Global surface temperature will increase by 1.0-3.7°C and the CO₂ concentration will rise to 730-1000ppm by the end of the 21st century. Furthermore, changing climate will lead to drought, water scarcity and reduced renewable water resources (IPCC, 2014). These changing environmental factors will influence plant functioning and physiological plant status. In the future, plants will experience heat and water stress with an increased intensity. As a result, ecosystem functions and agricultural yield are threatened (Gray and Brady, 2016). Referring to Gago et al. (2014), there will be an increased demand for food and water due to the exponential growth of mankind.

Environmental stress impacts, like the rising CO₂ concentration, temperature and drought events, lead to various responses within and between plant species (Gray and Brady, 2016). Fundamentally affected by the influence of changing environmental factors is plant photosynthesis (Flexas et al., 2014). Photosynthesis is crucial for CO₂ assimilation (Willey, 2016), plant growth (Damm et al., 2015), productivity (Tkemaladze and Makhshvili, 2016) and transpiration (Aroca, 2012). Environmental factors like the air temperature, CO₂ concentration in the atmosphere and the availability of light, nutrients and water influence plant photosynthesis (Flexas et al., 2012). Especially protein complexes (photosystems, ATP-synthase and cytochrome-*b₆f*-complexes) which contribute to photosynthesis are highly affected by abiotic stressors. Depending on plant type, time and the duration of the environmental stressor each plant reacts in a different way. Rapid stress responses and adaptations of the plant metabolism are crucial for plant survival in a changing environment (Nouri et al., 2015). Therefore, ongoing climate change will pose a significant threat to plant species because not all of them will be able to adapt (IPCC, 2014).

Under favourable environmental conditions, plants absorb light energy by photosynthetic pigments in photosystems (Raven et al., 2006). Spermatophytes and ferns termed as higher plants (Zwahr, 2006) have two different photosystems, photosystem I and photosystem II (Porcar-Castell et al., 2014). Photosystem I (PSI) has its absorption maximum at 700nm and photosystem II (PSII) at 680nm. Both photosystems operate simultaneously and continuously together. They contain chlorophyll molecules which absorb light energy and transfer it to the reaction centre. In turn, the reaction centre converts the light energy into chemical energy (Raven et al., 2006). This chemical energy is used to synthesize organic molecules from CO₂ and water (Alberts, 2005). Referring to (Canarache et al., 2006) this process is termed photosynthesis.

Indirect estimations of photosynthetic rates or photosynthetic related parameters are used to measure photosynthesis by remote sensing of fluorescence or reflectance of vegetation (Flexas et al., 2012). Common remote sensing approaches monitor global vegetation by means of vegetation indices (VIs), which make use of reflectance measurements in the visible and near-infra-red spectrum. The measured reflectance signal at the sensor is influenced by reflectance, transmission and ab-

sorption of the vegetation and atmospheric interactions. Consequently, the reflected signal varies with vegetation type and condition at different wavelengths (Lillesand et al., 2008). Although VIs have proven to deliver information about biomass, chemical composition, seasonal phenology and stress detection (Peñuelas and Filella, 1998) they are not directly related to photosynthesis (Flexas et al., 2012). Therefore, time series of derived VI parameters, like the chlorophyll content or leaf area index (LAI) are applied to estimate photosynthesis (Malenovsky et al., 2009). Nevertheless, a new approach in remote sensing enables the measurement of photosynthesis directly through the acquisition of sun-induced chlorophyll fluorescence (SIF) as a direct indicator of photosynthetic efficiency (Rascher et al., 2015). According to Cogliati et al. (2015), SIF is a slight signal in the visible and near-infra-red spectrum, dissipated by the photosynthetic apparatus of plants during photosynthesis (Grace et al., 2007). An excited chlorophyll molecule within the photosynthetic apparatus can dissipate its energy through four different ways: (1) radiation-free conversion, (2) fluorescence, (3) resonance energy transfer and (4) photooxidation (Voet et al., 2010). Because these dissipation pathways compete with one another (Atherton et al., 2016), detection of SIF can provide new insights to plant functioning and photosynthetic activity (Cogliati et al., 2015). In contrast to VIs, SIF can detect actual photosynthetic changes which are not restricted to the greenness of vegetation. In addition, SIF can be acquired at various spatial scales (Rascher et al., 2015) by using passive and active measurement techniques (Ač et al., 2015). Active measurement techniques are used at leaf-level scale, whereas passive measurement techniques can be used at leaf to canopy level. Active measurement techniques were most notably applied to understand plant mechanisms (Cendrero-Mateo et al., 2016). Passive measurement techniques use the spectral range between 600 to 800nm (Damm et al., 2015) to retrieve SIF at the two peaks around 685nm and 740nm (Rossini et al., 2015) because both peaks are located either near two Fraunhofer lines (680nm and 760nm) or the atmospheric O₂-A and O₂-B absorption bands (Joiner et al., 2016). In fact, the measured radiance signal consists of the reflected and fluorescent signal (Rascher et al., 2009). Thus, the fluorescence signal has to be decoupled from reflectance (Zarco-Tejada et al., 2012).

However, direct detection of photosynthetic activity is impeded, due to a missing satellite system dedicated to its measurement (Rascher et al., 2015). To remedy this shortcoming, the European Space Agency (ESA) plans to launch the FLuorescence EXplorer (FLEX) satellite within the 8th Earth Explorer mission, which explicitly monitors SIF at a spatial resolution of 300m within a spectral range of 500-880nm (Cogliati et al., 2015). Referring to the ESA (2015a), FLEX will help to fill current knowledge gaps in areas relating to ecosystems and the carbon cycle, agricultural management, vegetation productivity, sustainable development and health or stress of vegetation.

Recently, a few satellite systems were used to produce global SIF maps (Guanter et al., 2012; Frankenberg et al., 2011) and the detection of vegetation stress at canopy scale through SIF was demonstrated in various studies (Damm et al., 2010; Rossini et al., 2015). Empirically, high correlation between SIF and gross primary production (GPP) was detected as well as the early manifestation of SIF signals in vegetation stress (Yoshida et al., 2015). Nevertheless, interpretation of SIF is

challenging because it relies on the detailed knowledge of underlying plant processes (Mohammed et al., 2014). Consequently, there is a need to fill these knowledge gaps. To achieve this, more field studies with different abiotic and biotic stressors must be conducted under natural conditions which aim to evaluate the quantification of photosynthetic activities in a changing environment. Additionally, there is call for more experiments with different plant functional types and combinations of different stressors.

In this study, three different abiotic stress experiments (light, heat and water) with two different functional plant types (C_3 and C_4) were carried out. The aim was to evaluate stress detection of SIF in plants under different environmental conditions with the hypothesis that SIF can, in contrast to conventional VIs, add value to the detection of plant stress responses and provide insights to the underlying process understanding. The plant stress responses were acquired with a Hyperspectral Plant Imaging Spectrometer (HyPlant). HyPlant was developed by the Jülich Research Centre and the Finnish company Specim for passive monitoring of SIF and uses the approaches of the planned FLEX mission to provide valuable information about plant fluorescence retrieval (ESA, 2014b). The SIF signal was retrieved at 680nm (SIF₆₈₀) and 760nm (SIF₇₆₀) by means of the improved Fraunhofer Line Discrimination (iFLD) module proposed by ESA (2014a). In addition, the SIF plant stress responses were compared to several VIs and located within a bi-dimensional parameter space.

2 Background

2.1 Photosynthesis

Plant photosynthesis is important because its efficiency determines the quantity of the produced biomass. Oxygen-evolved plants use photosynthetic active radiation (PAR) efficiently in the solar spectral range of 400 to 700nm, which accounts for 48.7% of the total incident solar energy. Due to reflectance and transmittance (-4.9%), photochemical inefficiency (-6.6 %), energy losses through charge separation and carbohydrate biosynthesis (-30.9% in C₃ and -31.3% for C₄ plants), as well as respiration (-1.9% in C₃ and -2.5% in C₄ plants) and photorespiration in C₃ plants (-6.1%), only 4.6% of the total available solar radiation is used by C₃ plants and only 6.0% by C₄ plants (Zhu et al., 2010).

Plant photosynthesis is initiated by the absorption of light and can be split up into light and carbon fixation reactions. The light reaction transforms electromagnetic energy into chemical energy, whereby the carbon reactions use the previously produced chemical energy and atmospheric CO₂ to generate carbohydrates (Porcar-Castell et al., 2014). Light energy is mainly absorbed by photosynthetic pigments located inside of chloroplasts. Chlorophyll and carotenoids are the major photosynthetic pigments, whereby chlorophyll absorbs light in the red and blue visible spectrum and carotenoids in a spectral range of 400 to 500nm (Alberts, 2005). These spectral characteristics are used by VIs to determine vegetation pigments and biomass (Peñuelas and Filella, 1998). Both, chlorophyll and carotenoid pigments are part of antennae complexes (Scott, 2008). Several hundred chlorophyll molecules within the antennae complexes capture the electrons of light energy and transfer them to the adjacent reaction centre. The reaction centre contains a pair of chlorophyll *a* molecules, which trap the energy and excite the electron (Alberts, 2005). Consequently, the excited electron is captured by an electron acceptor molecule oxidizing the chlorophyll molecule (Raven et al., 2006).

Higher plants have two different photosystems, photosystem I (PSI) and photosystem II (PSII) (Porcar-Castell et al., 2014), whereby PSI reduces nicotinamide adenine dinucleotide phosphate (NADP) and PSII oxidises water (Scott, 2008). According to Voet et al. (2010), both photosystems are located in the thylakoid membrane, but excited independently of each other though they are serially connected. As a result, the electrons always flow from PSII to PSI. PSI has a higher content of chlorophyll *a* molecules in contrast to PSII which results in different spatial, spectral and temporal light absorption. In addition, PSII shows dynamic responses to environmental changes because most regulatory mechanisms are located there (ESA, 2015*b*). As reported by Porcar-Castell et al. (2014) the photosynthetic pigments of the reaction centres are termed P680 and P700 because PSII has its maximum light absorption at 680nm and PSI at 700nm, respectively. Since fluorescence measurements use emission bands around 680 and 740nm, it is assumed that most fluorescence arises from PSII because fluorescence intensity is increased at higher wavelengths (740nm) due to

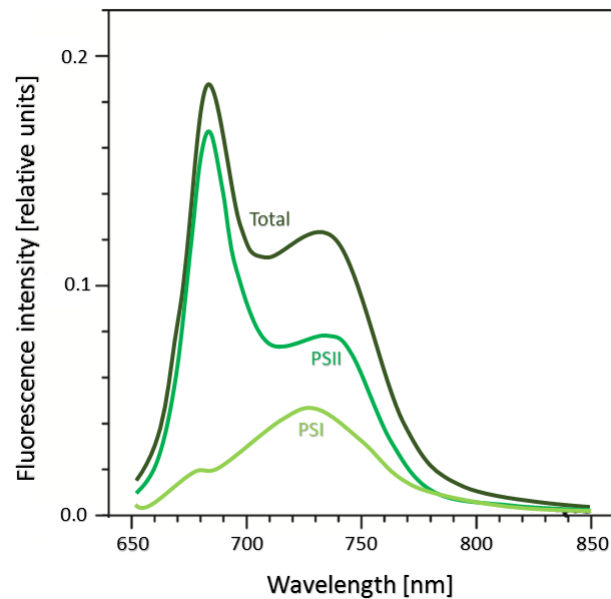


Figure 1: Fluorescence intensity of PSI and PSII to the total fluorescence intensity contribution (adapted from Porcar-Castell et al., 2014).

re-absorption within shorter wavelengths (680nm). Further, the PSI fluorescence spectrum overlaps with the PSII spectrum (Figure 1). Under minimal fluorescence state, PSI exhibits a maximum fluorescence peak around 720nm and PSII around 685nm (Franck et al., 2002). However, depending on the measurement method, spectral region, plant species and condition, PSI fluorescence contributes between 0 and 50% to the total fluorescence. In fact, the contribution of PSI is highest in the near-infra-red region whereby the contribution of PSII is highest in the red region (Porcar-Castell et al., 2014). Nevertheless, most physiological mechanisms are regulated on PSII and thus, functional stress responses will have a greater impact on the SIF₆₈₀ signal (Rascher et al., 2015).

When a chlorophyll molecule absorbs light energy it gets excited. In order to dissipate this energy, the chlorophyll molecule use four different strategies. It can create heat through radiation-free conversion, emit photons through fluorescence, transfer energy through resonance or transfer electrons through photooxidation (Voet et al., 2010). Energy transfer through resonance is also referred to as non-photochemical quenching (NPQ) and constitutes the most rapid way of responding to high light intensity (Willey, 2016). Because NPQ competes with fluorescence and photosynthetic activity (Ač et al., 2012), an increase in NPQ leads to a decline in photosynthetic and fluorescence yield (Mohammed et al., 2014). Several studies proved that this decline in fluorescence can be detected within fluorescence measurements (Franck et al., 2002; Kautsky and Hirsch, 1931; Murchie and Lawson, 2013; Trubitsin et al., 2015). Nevertheless, the process of photooxidation occurs during photosynthesis, as an excited chlorophyll molecule from PSII transfers its electrons via pheophytin, quinone A (Q_a) and B (Q_b) to the cytochrome- b_6f -complex. The cytochrome- b_6f -complex transfers the electrons to PSI and pumps protons into the thylakoid lumen generating a proton gradient.

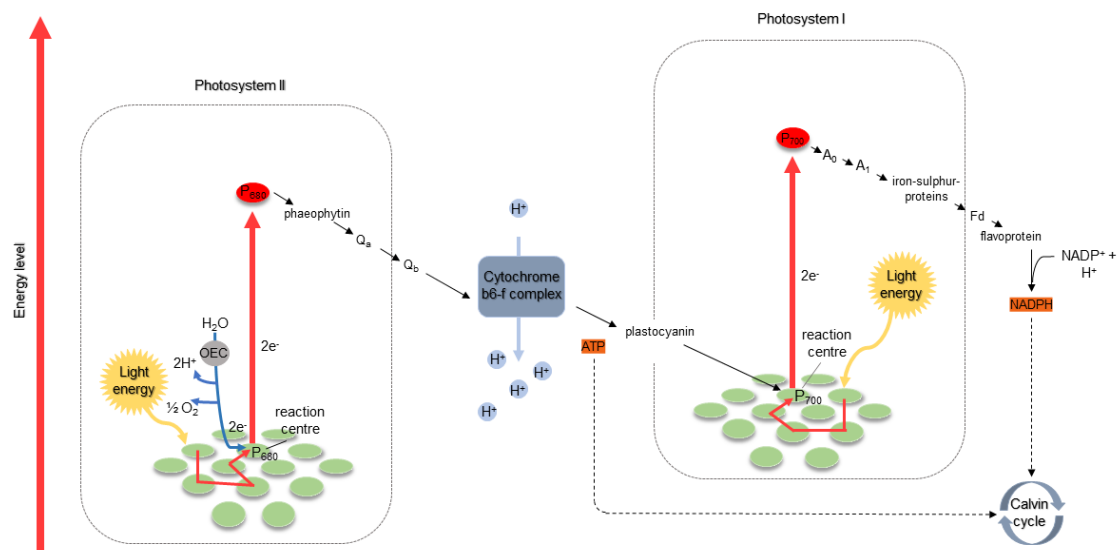


Figure 2: Linear electron transport of the photosynthetic light reaction. Red arrows signify the absorbed light energy, which excites PSI and PSII and the black arrows indicate the downhill electron transport chain by carrier molecules (adapted from Raven et al., 2006).

The resulting proton gradient is used by adenosine triphosphate (ATP) synthase complexes, which pump protons back into the chloroplast stroma. Additionally, absorbed energy by PSII is used by the oxygen evolving complex (OEC) to split water into electrons, protons and oxygen. Simultaneously, P700 absorbs light energy, transferring it from the primary acceptor molecule (A_0) to phylloquinone (A_1), ferredoxin (Fd), ferredoxin nicotinamide adenine dinucleotide phosphate reductase and finally to the co-enzyme $NADP^+$. $NADP^+$ is reduced to NADPH and P700 is oxidized by electrons (Porcar-Castell et al., 2014; Raven et al., 2006; Voet et al., 2010). This electron transfer is referred to as linear electron transfer (LET) (Porcar-Castell et al., 2014) and represents the light reaction of photosynthesis (Raven et al., 2006). Figure 2 illustrates a schematic representation of the linear electron transport at different energy levels.

In addition to the linear electron transport, a cyclic electron transport (CET) exists. Within this process, PSI works independently of PSII (Raven et al., 2006). Electrons from PSI are transferred to electron acceptor molecules around PSI, returning to the reaction centre of PSI while protons are pumped into the thylakoid lumen. The energy of the proton potential is used for ATP-synthase. As a result, CET generates only ATP rather than NADPH. CET is crucial to the initiation of photosynthetic dark reaction (Calvin cycle), modulation of NPQ and protection of PSI against light damages (Porcar-Castell et al., 2014).

The Calvin cycle uses the previously produced ATP and NADPH of the light reaction for carbon fixation. Start and product of the Calvin cycle is a sugar named Ribulose-1,5-bisphosphate (RuBP).

The enzyme Ribulose-1,5-bisphosphate carboxylase/oxygenase (Rubisco) catalyses the first reaction of the Calvin cycle generating a molecule with either three or four carbons. As a consequence, this first product of the Calvin cycle defines if a plant is either a C₃ or C₄ plant. Additionally, Rubisco plays an important role as it is the most common enzyme worldwide and accounts for approximately 40% of the total soluble proteins of leaves (Raven et al., 2006). Rubisco has a low affinity to CO₂ when a high amount of O₂ is available, leading to water losses as plants (especially C₃ plants) promote gas exchange. If a higher amount of O₂ relative to CO₂ is available, Rubisco conducts photorespiration in C₃ plants, which is an expensive process since it uses photosynthetic energy and yields neither ATP nor NADPH. During this process plants consume up to 50% of their photosynthetic fixed carbon and re-oxidising it to CO₂. This consequently leads to a reduction of photosynthetic activity and ultimately fluorescence (Flexas et al., 2012). The process of photorespiration is increased at high temperatures and dry conditions. Photorespiration is suppressed by C₄ plants (Zhu et al., 2010) because C₄ plants evolved primarily in tropical regions. Therefore, they solved the problem of photorespiration by a different anatomy. This anatomy comparts the Calvin cycle and the C₄ metabolism maintaining a high ratio between CO₂ and O₂ (Raven et al., 2006).

2.2 Abiotic plant stress responses

Photosynthetic efficiency plays an important role because a high photosynthetic efficiency is fundamental in ensuring food security. Photosynthetic efficiency is influenced by abiotic factors, particularly CO₂, light, temperature and water (Libbert, 1987), but equally so by biotic factors, plant development stage and the duration of stress (Feller and Vaseva, 2014). As a result, stress responses can fluctuate within species under equal environmental conditions due to physiological characteristics (Libbert, 1987).

Within this master thesis, plant stress is defined as an environmental factor that influences the fitness of plants (Willey, 2016). The following sections deal with physiological plant responses to light, heat and water stress with respect to the stress duration. Referred to Willey (2016), short-term responses particularly trigger biochemical and structural, whereby long-term responses affect anatomical and morphological plant stress responses. Main stress responses are carried together in Table 1.

2.2.1 Heat stress responses

Temperature is the determining factor of plant distribution and survival (Yamori et al., 2014) due to high spatial and temporal variability on the Earth's surface. Plants have different temperature ranges, which affect plant growth, phenology and photosynthesis. These temperature ranges can also vary between species and populations (Willey, 2016). For instance, the optimum temperature for maximum photosynthetic rates in C₃ plants lies between 10 and 35°C and in C₄ plants between

Experiment	Short-term [s-days]	Long-term [>days]
Heat	Destruction of biomolecules Increased CET Accumulation of HSPs Increased photorespiration Reduction of photosynthesis Inactivation of Rubisco activase Increased evaporation	Earlier anthesis Impact on plant development & growth Anatomical & morphological adaptations
Light	Chloroplast movement Damage of PSI & PSII Increased fluorescence & NPQ Alteration of leaf position Increased photoinhibition Changes in pH Increase of xanthophyll pigments	Accumulation of photoprotective pigments Anatomical & morphological adaptations
Water	Alteration in ABA concentration & process cascades Changes in aquaporin expression Accumulation of ROS Accumulation of solutes Increased stomatal closure	Enhanced root growth Accelerated senescence Anatomical & morphological adaptations

Table 1: Summary of abiotic short-term and long-term stress responses (Cechin, 1998; Edreva, 2005; Feller and Vaseva, 2014; Flexas et al., 2012; Nouri et al., 2015; Pastenes et al., 2004; Scott, 2008; Sztatelman et al., 2010; Willey, 2016; Yamori et al., 2014).

30 and 40°C. Deviations from this optimum temperature range reduce or inhibit photosynthesis (Yamori et al., 2014).

As described by Flexas et al. (2012), temperature stress cannot only be induced by air temperature but also by heat flecks. Heat flecks describe the rapid heating of leaves which affects leaf temperature. As a result, heat flecks can increase leaf temperature by up to 10°C. Heat flecks occur due to sunlight exposure or heat balance changes of the leaf. The production of zeaxanthin is a possible mechanism to protect leaves against heat flecks.

Plants experience temperature by physical changes of biomolecules and not through chemical receptors. Biomolecules operate at full capacity at specific energy levels and any deviations of this can lead to dysfunction. Thus, temperature stress has a direct impact on plant molecules because it alters physical properties. Consequently, temperature affects the structure of enzymes, lipids, nucleic acids and proteins. In contrast to small changes these fundamental changes are mostly irreversibly and fatal. Because membranes are built up of lipids, the thylakoid membrane structure is affected by temperature, which changes membrane fluidity (Willey, 2016). This can lead to a leaky membrane, altering pH. As a result, plants can induce heat shock proteins (HSPs) to protect membrane function and photosynthetic processes (Flexas et al., 2012).

One of the first temperature responses of plants is a lower photosynthetic rate because of Rubisco. There are two possible responses in relation to Rubisco with increasing temperature. One response concerns the heat labile Rubisco activase (Flexas et al., 2012). Rubisco activase is the activation enzyme of Rubisco moving inhibitory molecules off the catalytic sites (Gray and Brady, 2016). Rubisco activase can be inhibited by temperatures above 30°C, whereby Rubisco itself increases its activity

with increasing temperature being heat stable up to 50°C (Feller and Vaseva, 2014). Thus, the other possible temperature response refers to increasing Rubisco activity with higher temperature which leads to higher photorespiration rates (Flexas et al., 2012; Willey, 2016). The consequent reduction in photosynthetic efficiency of both possible responses is manifested in lower SIF values (Mohammed et al., 2014). Nevertheless, according to Feller and Vaseva (2014) an increased photorespiration occurs only in C₃ plants but not in C₄ plants. Another heat stress response is, according to Willey (2016), an increase in CET around PSI which activates NPQ by lowering pH in the thylakoid lumen. This stress response is important because it dissipates excess energy through NPQ. Nevertheless, referring to Scott (2008), a simple short-term strategy to lower heat stress is the movement of leaves reducing solar irradiance and thus heating effects. This can even include rolling of leaves.

Long-term responses affect mainly leaf anatomy, phenology, earlier anthesis, plant development and growth. Leaf anatomy depends not only on temperature but also on water availability. Leaves, which are exposed to hot and wet conditions have a large leaf area and a small volume releasing heat through evaporation. In contrast, plants in dry and hot areas exhibit a low ratio between surface area and volume reducing water loss. Additionally, a lot of plants in these hot and dry environments have reflective hairs, spines or wax on their surfaces to reduce heating (Willey, 2016). Further, heat acclimation of plants leads to a higher amount of saturated fatty acids within the membrane protecting its fluidity (Scott, 2008).

2.2.2 Light stress responses

Sunlight is important for plants because it provides energy for photosynthesis and thus life (Campbell et al., 2006). But excess light disrupts plant development and production (Edreva, 2005). Nevertheless, solar irradiance is one of the most varying factor over time and space (Flexas et al., 2012). Thus, plants must deal with varying PAR and dark-light transitions on a daily basis. These altering light conditions are often the result of atmospheric and canopy influences, as well as sun flecks (Willey, 2016). According to Flexas et al. (2012) sun flecks are leaf areas with a high temporal solar irradiance, analogous to heat flecks. Consequently, plants evolved strategies to use light energy to their advantage to ensure their survival (Ruban, 2015).

Dark-adapted plants exhibit a progressive increase in photosynthesis when abruptly illuminated. This photosynthetic increase lasts for several minutes until it reaches a steady-state level. Already induced leaves significantly lower their photosynthetic response to illumination. In addition to the photosynthetic increase of dark-adapted leaves under sudden light exposure a distinct increase of SIF occurs within seconds. Afterwards SIF decreases until it reaches a steady-state level based on the increase of photochemical quenching and non-photochemical mechanisms. It lasts about 20 minutes until SIF reaches steady state. This described SIF response to dark-adapted leaves is known as Kautsky effect. The Kautsky effect was successfully detected with active fluorescence measurements. However, these responses are crucial for daily photosynthesis in the understory and sun flecks (Flexas et al., 2012).

Referring to Willey (2016), the increased PSII activity creates a surplus of protons in the thylakoid lumen leading to pH changes and NPQ. NPQ is the result of xanthophyll pigment interconversion. The interconversion occurs between violaxanthin and zeaxanthin, whereby violaxanthin occurs at lower pH values and emits light energy while zeaxanthin dissipates light energy as heat at higher pH values. When plants are exposed to excess light, photosynthetic inhibition occurs because PSI and PSII complexes get damaged. PSII complexes, in contrast to PSI complexes, exhibit higher damage frequency. In fact, some PSII complexes get damaged at any irradiance. Referring to Mohammed et al. (2014) photodamage can be detected by increasing fluorescence values.

Another daily light stress response is chloroplast movement within cells. Chloroplasts can change their position very quickly depending on light conditions. Under high light (blue light) intensities, chloroplasts move to the opposite cell walls (avoidance response) whereas under low light intensities the chloroplasts move to the cell walls directly oriented to light incidence (accumulation response). As a consequence, maximum photosynthesis can be achieved under low light intensities and photoinhibition can be prevented under high light intensities (Sztatelman et al., 2010). Additionally, Pastenes et al. (2004) reported leaf movement as a function of the light regime. Thus, the leaf position can be directional or non-directional to solar irradiance, altering photosynthetic yield.

Adaptation to high light intensities and UV radiation include photoprotective pigments like anthocyanins, flavonols and carotenoids. These pigments are more than photoprotective shields for chloroplasts as they have antioxidant and ROS(reactive oxygen species)-scavenging activities, which protect the photosystems from overexcitation and photooxidative stress (Edreva, 2005). These photosynthetic pigments are not only visible to the eye, they can also be detected by VIs. Furthermore, leaves developed structural responses like waxiness or pubescence, profound palisade mesophyll layers and elongated palisade cells which contain a high amount of chlorophyll (Willey, 2016).

2.2.3 Water stress responses

Based on the fact, that all terrestrial plants descend from freshwater algae, water constitutes the most crucial factor (Willey, 2016). Water availability is vital because it controls crop yield and limits ecosystem productivity (Gray and Brady, 2016). However, drought occurs mostly in combination with salt, light and temperature stress, which impedes distinguishing between them (Flexas et al., 2012).

Within seconds, plants close their stomata in response to water in an attempt to reduce water loss (Willey, 2016). Consequently, less CO₂ can be acquired by chloroplasts, limiting photosynthesis (Nouri et al., 2015). This is accompanied by changes in protein and membrane interactions as well as diurnal changes in aquaporin expression. Aquaporins are proteins within membranes, which mediate water transport through plant cells (Willey, 2016). Furthermore, Rubisco is vulnerable to water stress and decreases activity with increasing water stress (Flexas et al., 2012) reducing the Calvin cycle activity (Cechin, 1998).

Water stress can lead to irreversible damages of photosynthetic apparatus and speed up leaf senescence (Flexas et al., 2012). Both, plant tissue death and leaf senescence are detectable with VIs be-

cause they reduce green biomass (Hill, 2013). Furthermore, water stress is lethal to plants when they are not able to adapt. One adaptation is the mediation of water stress responses by abscisic acid (ABA). Water deficit increases the ABA concentration in cells, which reduces the negative water potential in combinations of anions (Cl^- , NO_3^-) and cations (Ca^{2+} , K^+) the negative water potential (Willey, 2016). In addition, ABA controls stomatal closure, preventing water loss through transpiration (Feller and Vaseva, 2014). Gray and Brady (2016) reported that plants suffering under water stress shift their resource investment from shoots to roots resulting in root elongation and shoot growth stop. This response was also linked to ABA concentration. Consequently, ABA induces gene expression and changes plant physiology in water stressed plants (Willey, 2016). But excessive ABA concentration in chloroplast cells inhibit photosynthesis leading to plant tissue death as described by Scott (2008).

Under reduced water availability plants are unable to use ATP and reduction equivalents in a seemly way, accumulating ROS. ROS act as signalling molecules but pose a significant threat to plants because they initiate plant senescence and death when ROS are not detoxified by enzymes. ROS get extremely important when light, heat and water stress occur in combination (Feller and Vaseva, 2014).

A temporary respite of water stress can be achieved through altering plant metabolism by accumulation of solutes like sugars or amino acids. These solutes are non-toxic and adjust the osmotic potential of the cells, maintaining cell water inflow (Scott, 2008). During drought periods, some plants produce waxy substances on their leaves, reducing transpiration. But the waxy layers on the leaves are not or only partially reversible after drought, challenging plant functioning (Feller and Vaseva, 2014). Plants, which are adapted to water stress developed highly specialized anatomical and morphological adaptations, maximising nutrient and water use efficiency. However, changes in leaf anatomy and morphology are the most significant adaptations. Leaves developed special forms of stomata like crypts or grooves, leathery and long-lived leaves and decreased stomata densities. Additionally, some leaves roll downwards reducing water loss through stomata. Some species developed water storing tissues or are even tolerant against desiccation (Willey, 2016).

3 Methods

3.1 Study Areas

The experimental sites are located within two different regions in the Western part of Germany (Figure 3). The heat and light experiments were conducted within the study area of the Campus Klein-Altendorf (ESA, 2016a) whereby the water experiment was carried out within the Rur catchment (ESA, 2013). Both study areas are used as research sites of the Transregional Collaborative Research Centre 32 (TR32) (ESA, 2016a). The TR32 is a collaborative project of the nearby Research Centre Jülich and the University of Aachen, Bonn and Cologne, with the aim of understanding the soil-vegetation-atmosphere system in a deeper qualitative and quantitative manner (TR32, 2017).

The Campus Klein-Altendorf is situated near Bonn and Meckenheim. It is characterized by an Atlantic climate, mainly influenced by south-western winds on the lee side of the Eifel. Average

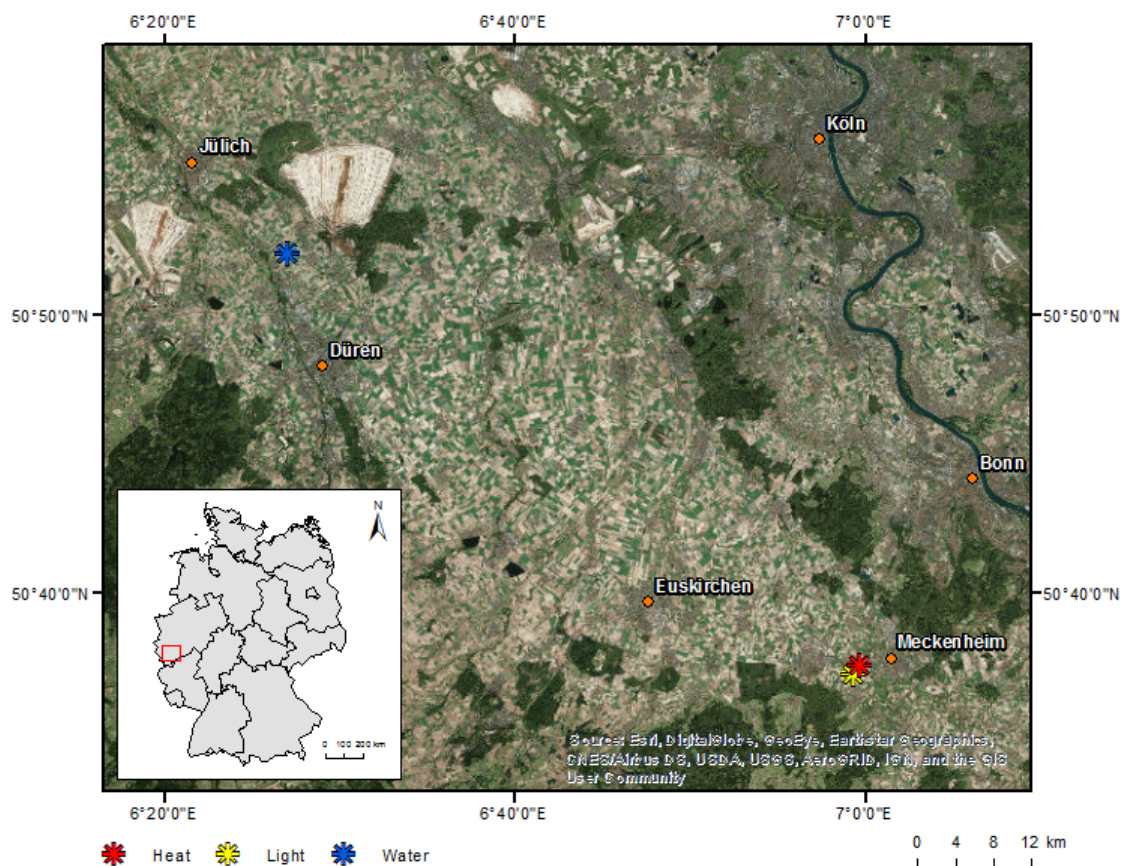


Figure 3: Study areas and experimental sites. The pins are coloured by the three different experiments. The heat experiment is coloured in red, the light experiment in yellow and the water experiment in blue, respectively.

annual temperature is 9.4°C and the average annual precipitation is 603mm. The study site contains a total agricultural area of 181ha with barley, sugar beet and wheat as dominant crop types (Campus Klein-Altendorf, 2010).

The Rur is a tributary of the Maas and forms a 2'354 km² catchment in Western Germany with small extending areas to Belgium and Netherlands (ESA, 2013). The mean annual precipitation in the Rur catchment is approximately 700mm and the annual temperature 11°C (Wieneke et al., 2016). The Rur catchment can be divided into a northern and a southern part, whereby the bedrock of the Eifel mountains is covered by sedimentary rocks with low groundwater storage while the northern part exhibits soils which evolved from loess (Montzka et al., 2013). In addition, the northern part receives in contrast to the southern part a relative low amount of precipitation (Ali et al., 2015). The northern part exhibits intensive agricultural areas and urbanization and the southern part of the catchment has several drinking water reservoirs (ESA, 2013). The study area around Selhausen exhibits, according to Ali et al. (2015), a highly variable soil surface water content due to underlying sediments and a weak inclination (< 4°) in the east-west direction. Maize, potatoes, rapeseed and sugar beet are the dominant crop types (Wieneke et al., 2016).

3.2 Experiments

3.2.1 Heat stress

The heat stress experiment was conducted near the research station of the Campus Klein-Altendorf during a naturally occurring heat wave in Germany in 2015 (ESA, 2016a). A naturally occurring heat wave is defined as a period of several consecutive days with abnormally high surface temperatures (Rafferty, 2015). The heat wave in Germany 2015 started on July 1st 2015 and lasted about 5 days (Yang et al., in review). The first acquisition took place before the heat wave started on June 30th 2015 at 3:51 p.m. local time with the air temperature reaching 26.6°C. The second acquisition happened during the heat wave on July 2nd 2015 at 3:16 p.m. local time and an air temperature of 33.7°C (Vilfan et al., 2016). Both measurements were acquired at a flight altitude of 350m above ground and a spatial resolution of 0.5 x 1m (ESA, 2016a). The data was acquired for two different crop types, in particular three C₃ crops (barley, rapeseed, wheat) and one C₄ crop (corn) (Yang et al., in review).

3.2.2 Light stress

The light stress experiment was like the heat stress experiment, carried out near the research station of the Campus Klein-Altendorf during the heat wave on July 1st 2015. The data was acquired at 3:14 p.m. local time at a flight altitude of 350m above ground and a spatial resolution of 0.5 x 1m. The light stress experiment was based on a virtual cloud simulation with a 6x30m net, which was put 1.5m above a sugar beet field (50°37'3.77"N/ 6°59'19.20"E). The experimental set-up is illustrated in Figure 4. The net reduced incoming solar radiation by 50% and was laid over the sugar beet field



Figure 4: Experimental set up of the light experiment (Panigada et al., 2016).

for at least one hour. As a consequence, the sugar beet adapted to the reduced light condition. Half an hour before the aircraft passed, the net was removed continuously and slowly until the last two meters. These were rolled up rapidly and only seconds before the aircraft flew over (ESA, 2016a).

3.2.3 Water stress

The water experiment was conducted between Selhausen, Niederzier and Oberzier. The experiment was implemented on two sugar beet fields ($50^{\circ}52'28.45''\text{N} / 6^{\circ}26'58.07''\text{E}$ and $50^{\circ}51' 59.09''\text{N} / 6^{\circ}27'4.17''\text{E}$), which exhibit a well and a poor watered part on the field. As a consequence, water stressed and unstressed sugar beet were located on the same field (Figure 5). The data was acquired on August 23rd 2012 at an altitude of 600 m above ground in the North-South direction. The measurement was repeated at three local times (Central European Summer Time, CEST); two and a half hours before solar noon (11:50), at solar noon (13:30) and two and a half hours after solar noon (16:05) (ESA, 2013).



Figure 5: Water unstressed sugar beet is illustrated on the right side, whereas water stressed sugar beet is located on the left side (Damm, 2016).

Experiment	DOY	Year	Acquisition Time	Flight altitude	Spatial resolution
Heat	181	2015	15:51	350m	0.5x1m
	183	2015	15:16	350m	0.5x1m
Light	182	2015	15:14	350m	0.5x1m
Water	236	2012	11:56	600m	1x1m
	236	2012	13:50	600m	1x1m
	236	2012	16:05	600m	1x1m

Table 2: Acquisition details of each experiment. Acquisition time is denoted in CEST (ESA, 2016a, 2013; Vilfan et al., 2016).

3.3 HyPlant data acquisition and pre-processing

The data acquisition took place on four different days and two different years. Acquisition details of each experiment were summarized in Table 2. The data was acquired with the Hyperspectral Plant imaging spectrometer (HyPlant) sensor (illustrated in Figure 6) through a trained operator under very good atmospheric and weather conditions. The HyPlant sensor was mounted on a Cessna Grand Caravan C208B from the CAE Aviation company. The Research Centre Jülich developed the HyPlant sensor in collaboration with SPECIM Spectral Imaging Ltd (Finland). HyPlant is an airborne sensor, which is dedicated to the monitoring of vegetation (Figure 6). The development time lasted two and a half years and the resultant sensor is a composite of the following five components: (1) the Dual Channel VNIR and SWIR imager, (2) the Fluorescence imager, (3) the data acquisition and power unit, (4) the position and attitude sensor and (5) the adjustable mount (ESA, 2016a,b, 2013).

Both, the Dual Channel and the Fluorescence imager are push-broom sensors. The Dual Channel imager consists of two sensors, which provide spectral informations between 380 to 2500 nm with a common fore objective lens (Rascher et al., 2015). The lens has a spectral resolution of 3nm within the visible and near infra-red spectrum and a 10nm spectral resolution within the short-wave infra-red spectrum. The Fluo imager measures the at sensor radiance of the vegetation in a spectral range of 670-780nm. It provides data with a spectral resolution of 0.25nm within the spectral range of two oxygen absorption bands (O_2 -A and O_2 -B). The Dual and Fluo rack modules make up the data acquisition and the power unit. Both rack modules contain a data acquisition computer and software, the control electronic of the imager, a GPS/INS sensor and a power supply. Simultaneously to the image data acquisition, the GPS/INS sensor recorded altitude and position of the aircraft, which were used for geo-referencing and image rectification. The last component, the adjustable mount, allowed the alignment of the field of view from both the Dual and Fluo imagers (ESA, 2013).

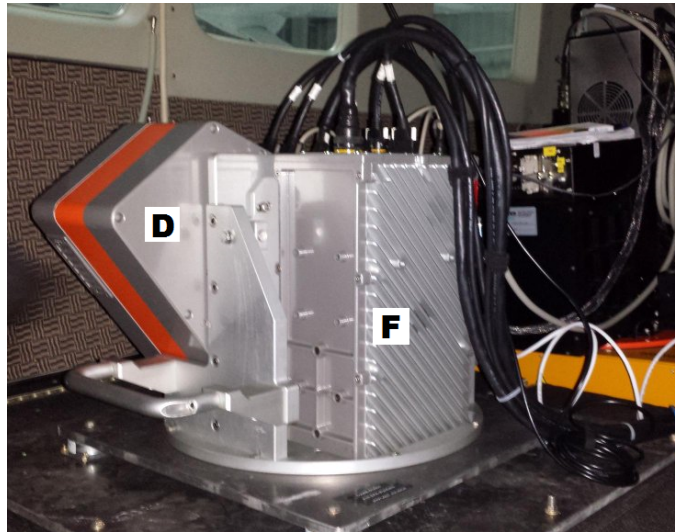


Figure 6: HyPlant sensor with the Dual (D) and Fluo (F) modules (adapted image from HyPlant, 2014).

3.4 Retrieval of vegetation indices and fluorescence

Dual raw data was geo-referenced with flight attitude and position. Afterwards it was radiometrically corrected and the at sensor radiance was rectified with calibration files provided by SPECIM. The radiometric calibration and geo-referencing were implemented with CaliGeo, while the atmospheric correction was performed using ATCOR. In a final step, top-of-canopy reflectance data was used to calculate vegetation indices in IDL. The simple ratio (SR) was calculated for all three experiments and eight additional VIs were calculated only for the heat stress experiment. Similarly, the Fluo raw data was radiometrically corrected and geo-rectified with calibration files delivered by SPECIM. Further, the Fluo data was deconvolved to correct the non-linear point spread function (ESA, 2016a).

3.4.1 Retrieval of vegetation indices

Referring to the ESA (2014a) the vegetation indices were specifically calculated for HyPlant data and defined either by a spectral range indicated by <xxx – xxx> or by a central wavelength \pm the range of the number of HyPlant bands. In the following, the calculated vegetation indices are shortly introduced by their formula and relevance. Additionally, they were subdivided into functional, structural and water indices. The functional VIs are related to functional plant processes (i.e. photosynthesis), the structural VIs to the anatomical structure (i.e. photochemical pigments) and the water VIs to the water content of plants. The Equation 1, 2, 3, 5 and 9 were taken from the ESA (2014a) and Equations 4, 6, 23 and 8 were calculated according to the ESA (2014a) with their central wavelength \pm the range of 4 bands.

Structural indices

The SR was introduced by Asrar et al. in 1984 (cited in ESA, 2014a). According to Sims and Gamon (2003), the SR is sensitive to the chlorophyll content of plants due to a strong chlorophyll absorption in the red spectral region.

$$SR = \frac{R_{<795-810>}}{R_{<665-680>}} \quad (1)$$

Tucker (1979) proposed the normalized difference vegetation index (NDVI), which is similar to the SR sensitive to chlorophyll content in green vegetation (Hill, 2013). Consequently, the NDVI correlates with biomass, the LAI and the condition of the observed vegetation. According to Carlson and Ripley (1997), the NDVI saturates at high LAI values.

$$NDVI = \frac{R_{<795-810>} - R_{<665-680>}}{R_{<795-810>} + R_{<665-680>}} \quad (2)$$

The enhanced vegetation index (EVI) was developed to measure biomass (Jiang et al., 2008) and is sensitive to canopy architecture, structural variations and types while avoiding saturation at high vegetation densities (Huete et al., 2002).

$$EVI = 2.5 * \left(\frac{R_{<795-810>} - R_{<665-680>}}{R_{<795-810>} + 6 * R_{<665-680>} - 7.5 * R_{<475-490>} + 1} \right) \quad (3)$$

Functional indices

According to Serrano et al. (2002), the nitrogen concentration in canopies can be estimated by the normalized difference nitrogen index (NDNI). Furthermore, the NDNI is not only an indicator for the amount of nitrogen but also for photosynthesis.

$$NDNI = \frac{\log\left(\frac{1}{R_{<1489-1534>}}\right) - \log\left(\frac{1}{R_{<1657-1702>}}\right)}{\log\left(\frac{1}{R_{<1489-1534>}}\right) + \log\left(\frac{1}{R_{<1657-1702>}}\right)} \quad (4)$$

The photochemical reflectance index (PRI) provides information about photosynthetic radiation use efficiency, pigment content and chloroplast movement. Especially, the reflectance signal at a wavelength of 531nm reveals information about xanthophyll cycle pigments (Gamon et al., 1997). Additionally, the PRI correlates with NPQ (ESA, 2014a) and serves as an indicator of water stress detection (Panigada et al., 2014).

$$PRI = \frac{R_{570\pm1} - R_{531\pm1}}{R_{570\pm1} + R_{531\pm1}} \quad (5)$$

Water indices

Originally, the moisture stress index (MSI) was proposed by Hunt and Rock (1989) and provides information about leaf water content. Further, the MSI is inversely related to equivalent water thickness in the canopy and non-linearly related to the NDII (Yilmaz et al., 2008).

$$MSI = \frac{R_{<1629-1674>}}{R_{<828-841>}} \quad (6)$$

Referred to Yilmaz et al. (2008) the normalized difference infra-red index (NDII) senses the equivalent water thickness of vegetation and was originally proposed by Hardisky et al. (1983).

$$NDII = \frac{R_{<828-841>} - R_{<1629-1674>}}{R_{<828-841>} + R_{<1629-1674>}} \quad (7)$$

The normalized difference water index (NDWI) measures the status of liquid water in vegetation, whereby green vegetation generally exhibits positive NDWI values. The NDWI increases with increasing fraction of vegetation area (Gao, 1996).

$$NDWI = \frac{R_{<854-867>} - R_{<1219-1264>}}{R_{<854-867>} + R_{<1219-1264>}} \quad (8)$$

Peñuelas et al. (1993) originally described the water band index (WBI). This water index provides information about the water content at leaf and canopy level. Additionally the WBI is able to differentiate seasonal water content of different vegetation types (Serrano et al., 2000).

$$WBI = \frac{R_{<955-970>}}{R_{<890-905>}} \quad (9)$$

3.4.2 Retrieval of fluorescence

The pre-processed at sensor radiance consisted of the reflected radiance and the emitted fluorescence of the vegetation (ESA, 2014a). Decoupling of the emitted fluorescence and the reflectance is challenging, though its signal constitutes only a small part of the received radiance signal (Zarco-Tejada et al., 2012). The fluorescence signal constitutes approximately 1-5% in the near infra-red and approximately 30% in the red spectral region to the received at sensor radiance. Nevertheless, passive SIF can be retrieved either in Fraunhofer lines or in atmospheric absorption bands, where solar irradiance is strongly attenuated by two telluric oxygen absorption bands at 687nm (O₂-B) and 760nm (O₂-A), respectively Meroni et al. (2009). Currently, a couple of algorithms to retrieve passive SIF exist, though the FLD (Fraunhofer Line Discrimination) approach serves as standard method (ESA, 2014a).

This study used the iFLD (improved Fraunhofer Line Discrimination) module developed by Alexander Damm and Francisco Pinto, by retrieving SIF at the O₂-A and O₂-B bands. The module is based on the 3FLD (modified Fraunhofer Line Discrimination) and the iFLD methods, which are enhanced methods of the standard Fraunhofer Line Discrimination (FLD) (ESA, 2014a). Initially, the FLD was proposed by Plascyk in 1975 (cited in Guanter et al., 2010) and relies on the decoupling of reflectance and fluorescence through the analysis of the measurements inside and outside the O₂-absorption bands (Meroni et al., 2009). Decoupling of the fluorescence and reflectance signals is possible due to a high contrast within the atmospheric oxygen absorption bands (ESA, 2013). The disadvantage of the standard FLD method is the assumption of a constant fluorescence and reflectance inside and outside the oxygen absorption bands (Damm et al., 2011), which leads to large sources of error (Alonso et al., 2014). Thus, the 3FLD and the iFLD methods provide an improved accuracy of the retrieved SIF (Damm et al., 2011).

The proposed iFLD module from Alexander Damm and Francesco Pinto allows the SIF retrieval of both, the O₂-A and O₂-B absorption bands, since six atmospheric parameters from MODTRAN5 (radiative transfer model) simulations are known (ESA, 2014a). They applied the MODTRAN interrogation technique from Verhoef and Bach (2003) to determine the following six atmospheric parameters: (1) the direct atmospheric transmittance in the direction of the sun (τ_{ss}) and (2) of viewing (τ_{oo}), (3) the diffuse atmospheric transmittance for solar incidence (τ_{sd}), (4) the directional atmospheric transmittance for solar incidence (τ_{do}), (5) the top of the atmosphere bidirectional reflectance (τ_{so}) and (6) the spherical albedo of the atmosphere (ρ_{dd}). In order to obtain these six parameters, three model runs of MODTRAN5 were necessary with the assumptions of an uniform Lambertian surface reflectance and a flat surface albedo of 0%, 50% and 100%. Referring to the ESA (2014a) the following equations reveal the fluorescence and reflectance signals:

$$F_i = \frac{B \left[\frac{X_i(E_o + X_o \langle \rho_{dd}^o \rangle) - A * X_o(E_i + X_i \langle \rho_{dd}^i \rangle)}{B(E_o + X_o \langle \rho_{dd}^o \rangle) - A(E_i + X_i \langle \rho_{dd}^i \rangle)} \right]}{\langle \tau_{oo}^i \rangle + \langle \tau_{do}^i \rangle} \quad (10)$$

$$X_{i,o} = (L_{i,o}^{AtS} - \frac{\langle E_{i,o}^o * \cos \theta_{il} \rangle}{\pi} \langle \rho_{so}^{i,o} \rangle) \quad (11)$$

$$E_{i,o} = \frac{\langle E_{i,o}^o * \cos \theta_{il} \rangle}{\pi} (\langle \tau_{ss}^{i,o} \tau_{oo}^{i,o} \rangle + \langle \tau_{sd}^{i,o} \tau_{oo}^{i,o} \rangle + \langle \tau_{ss}^{i,o} \tau_{do}^{i,o} \rangle + \langle \tau_{sd}^{i,o} \tau_{do}^{i,o} \rangle) = [E_{i,o}^{dir} + E_{i,o}^{dif}] \quad (12)$$

$$R_i = A * R_o \quad (13)$$

$$F_i(\langle \tau_{oo}^i \rangle + \langle \tau_{do}^i \rangle) = B * F_o(\langle \tau_{oo}^o \rangle + \langle \tau_{do}^o \rangle) \quad (14)$$

$$A = \frac{R * \omega_1 + R_{right} * \omega_2}{R_{left}} \quad (15)$$

$$\omega_1 = \frac{\lambda_{right} - \lambda}{\lambda_{right} - \lambda_{left}} \quad (16)$$

$$\omega_2 = \frac{\lambda - \lambda_{left}}{\lambda_{right} - \lambda_{left}} \quad (17)$$

where R is the reflectance, λ_{right} and λ_{left} are the right and left wavelength shoulder of the reflectance at the O₂-absorption band λ , A is a linear 3rd order polynomial interpolation of λ_{right} and λ_{left} , B was set to 0.8, θ_{il} is the illumination zenith angle, $E_{i,o}$ the surface irradiance (diffuse and direct components) and the characters *i* and *o* stand for the position inside and outside the O₂-absorption band, respectively (ESA, 2014a).

Due to slight inaccuracies in the modelled atmospheric parameters and sensor acquisition errors (e.g. spectral shifts), the retrieved SIF exhibits slight miscalculations (Rascher et al., 2015). As a consequence, the Cr method and transmittance correction technique were applied (ESA, 2014a). The Cr method is used to retrieve the actual spectral shift and FWHM (Full Width at Half Maximum) of a high resolution spectrometer. In order to achieve this, MODTRAN reference spectra of different FWHM and variable spectral shifts are resampled until the perfect match between the measured

and the MODTRAN irradiance is found (Busetto et al., 2011). The Cr method used for HyPlant assumed a high correlation between the observed and simulated spectra and relied on a iterative cost function which maximized the Pearson correlation between both spectra (ESA, 2014a). The transmittance correction technique considers a non-fluorescent reference surface to compensate systematic errors. The non-fluorescent reference surface should exhibit zero fluorescence around the O₂ absorption bands resulting in a smooth reflectance signal. Aberrations of this reference were attributed to miscalculations, which were readjusted by a correction factor. The correction factor was applied to the up-welling transmittance (τ_{oo}) leading to zero fluorescence for non-fluorescent surfaces (Damm et al., 2014; Guanter et al., 2007, 2010).

3.5 Stress indicators

In order to evaluate plant functioning under light, heat and water stress, specific regions of interest (ROI) were selected within the processed dual and fluo images in ENVI. Each ROI contained several hundred pixels, except the ROI from stressed and unstressed sugar beet within the light experiment. These ROI consisted of thirty pixels because only the last two meters of the sugar beet field were light stressed. SIF and vegetation index data of the selected ROI was analysed in a statistical program (RStudio). In addition to the SIF₆₈₀ and SIF₇₆₀ values, the SIF ratio (SIF₆₈₀/SIF₇₆₀) was calculated. Referring to Lichtenthaler et al. (1998) the SIF ratio is inversely related to the chlorophyll content in leaves and an indicator of stress induced decrease in leaf chlorophyll content. The results of all stress indicators (SIF, VIs) were illustrated in boxplots and maps (Matlab).

In addition, the SIF data was illustrated in a bi-directional parameter space proposed by Mohammed et al. (2014). The bi-dimensional parameter space is defined by two SIF axes (Figure 7). The x-axis represents the ratio between unstressed to stressed SIF₆₈₀ values, whereby the y-axis is defined analogously with the SIF₇₆₀ values. When plants are not stressed, the mean value of the normalized SIF₆₈₀ and SIF₇₆₀ values should be 1, labelled as control. Originally, Mohammed et al. (2014) proposed the bi-dimensional parameter space with nitrogen (N_{lit}), temperature (T_{lit}) and water (W_{lit}) as stress types within a literature analysis. The mean values of the measured stress types are depicted as points and the standard deviations of the SIF ratios define the boxes around the mean values. Further, the intensity of plant stress response is indicated by a stress intensity fluorescence index (SIFI). The SIFI (red arrow) defines the distance between a measured point (X) with the coordinates of SIF₆₈₀(stressed:unstressed) and SIF₇₆₀(stressed:unstressed) and the coordinates of the control point. Mohammed et al. (2014) reported the following formula to calculate the SIFI:

$$SIFI = \sqrt{\left(\frac{FR}{FR_C} - 1\right)^2 + \left(\frac{FFR}{FFR_C} - 1\right)^2} \quad (18)$$

In this study, FR corresponds to SIF₆₈₀ and FFR to SIF₇₆₀ since FR refers to fluorescence measured

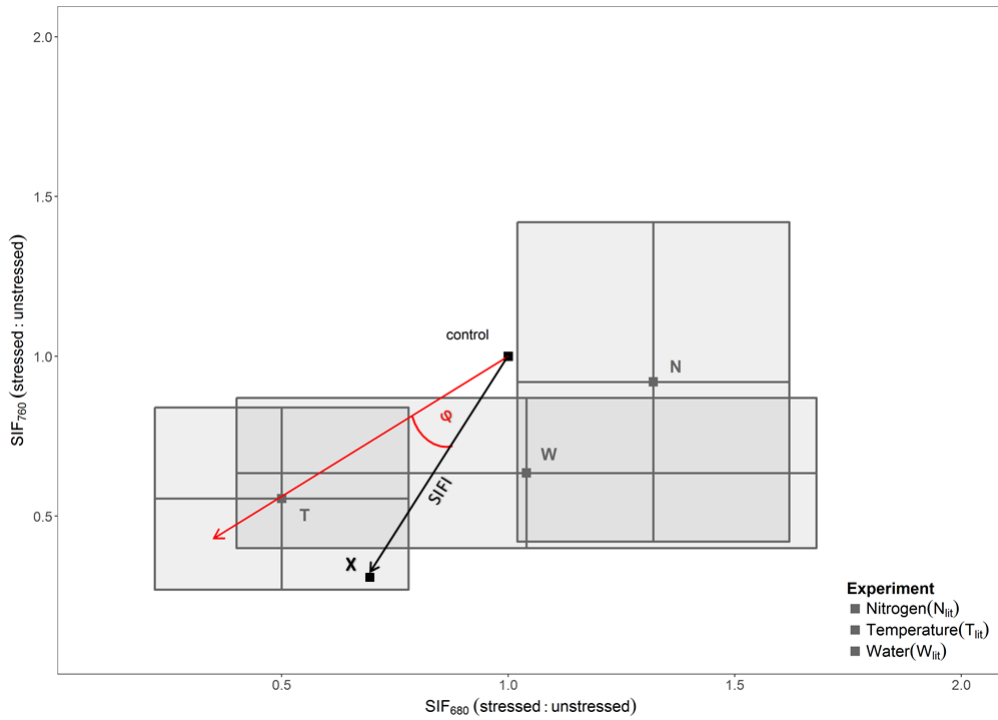


Figure 7: Adapted bi-dimensional parameter space from Mohammed et al. (2014).

in the red spectrum and FFR to fluorescence in the far-red spectrum. The direction of the SIFI and consequently the stress type is defined by the cosine angle (φ) between the control and the measured point. The cosine angle was defined as Stress Fluorescence Index (SFI) and named after the stress type. For instance, when temperature was the stress type, then the index was named TSFI (Temperature Stress Fluorescence Index). The SFI can range from -1 to 1, whereby 1 indicates that the measured point is fully stressed by the corresponding stress type and -1 indicates that the measured point is not stressed by the corresponding stress type. The SFI was calculated according to:

$$SFI = \frac{\left(\frac{FR}{FR_C} - 1\right)(T_{FR} - 1) + \left(\frac{FFR}{FFR_C} - 1\right)(T_{FFR} - 1)}{\sqrt{\left(\frac{FR}{FR_C} - 1\right)^2 + \left(\frac{FFR}{FFR_C} - 1\right)^2} \sqrt{(T_{FR} - 1)^2 + (T_{FFR} - 1)^2}}, \quad (19)$$

whereby T_{FR} and T_{FFR} were the coordinates from the mean values of the ratio between stressed and unstressed SIF_{680} and SIF_{760} , respectively. Consequently, T_{FR} and T_{FFR} from the temperature (TSFI) and water (WSFI) experiment were adopted from the meta-analysis from Mohammed et al. (2014).

Because the meta-analysis from Mohammed et al. (2014) was conducted without light as stress type, both parameters (T_{FR} and T_{FFR}) were calculated separately. Additionally, an average control value of SIF_{680} (FR_C) and SIF_{760} (FFR_C) from unstressed sugar beet was calculated. The resultant LSFI formula is:

$$LSFI = \frac{-1.052 + 0.054\left(\frac{FR}{FR_C}\right) + 0.999\left(\frac{FFR}{FFR_C}\right)}{\sqrt{\left(\frac{FR}{FR_C} - 1\right)^2 + \left(\frac{FFR}{FFR_C} - 1\right)^2}}. \quad (20)$$

The control values of the heat stress experiment were the ROI pixel values from the 30th June and the stressed values were from the 2nd July 2015 leading to the following TSFI formula:

$$TSFI = \frac{1.41 - 0.74\left(\frac{FR}{FR_c}\right) - 0.67\left(\frac{FFR}{FFR_c}\right)}{\sqrt{\left(\frac{FR}{FR_c} - 1\right)^2 + \left(\frac{FFR}{FFR_c} - 1\right)^2}}. \quad (21)$$

Like the control values of the light stress experiment, the control values of the water stress experiment were calculated by the average of unstressed sugar beet field but they were calculated for each sugar beet field and at each time. As a result, the WSFI formula is:

$$WSFI = \frac{0.885 + 0.109\left(\frac{FR}{FR_c}\right) - 0.994\frac{FFR}{FFR_c}}{\sqrt{\left(\frac{FR}{FR_c} - 1\right)^2 + \left(\frac{FFR}{FFR_c} - 1\right)^2}}. \quad (22)$$

4 Results

4.1 Heat stress

Airborne sun-induced chlorophyll fluorescence and vegetation index images from the study area are illustrated in Figure 8. It clearly illustrates the varying responses of the four different crops (barley, corn, rapeseed and wheat) during the heat wave in summer 2015.

4.1.1 Sun-induced chlorophyll fluorescence

Analysis of the heat stress data values are depicted as boxplots in Figure 9a-k. SIF_{680} values of all crops are illustrated in Figure 9a. The SIF_{680} values of barley, rapeseed and wheat decreased, whereby the SIF_{680} values of corn increased during the heat wave. Further, corn revealed the biggest difference in SIF_{680} values between the two acquisition dates. The values ranged from -0.2990 to $1.0311\text{mWm}^{-2}\text{nm}^{-1}\text{sr}^{-1}$. Wheat had the lowest positive SIF_{680} value, measured on the 2nd July and rapeseed the highest SIF_{680} value, measured on the 30th June 2015 (Figure 9a). This finding is also visible in Figure 8c and 8d, where rapeseed shows the highest SIF_{680} values. The SIF_{760} values showed equal responses like the SIF_{680} values. Figure 9b depicts the SIF_{760} values, which were higher than the SIF_{680} values and ranged from 0.5392 to $2.6748\text{mWm}^{-2}\text{nm}^{-1}\text{sr}^{-1}$. As with the SIF_{680} values, rapeseed showed the highest SIF_{760} value. Furthermore, barley showed the maximum decrease (-55%) between unstressed and stressed physiological status. In contrast, the lowest SIF_{760} value was measured in corn. Figure 8e and 8f illustrate the decrease and increase of the SIF_{760} values, respectively. Especially, the decrease of the SIF_{760} values in rapeseed is visible between both acquisition dates. Figure 9c displays the ratio between SIF_{680} and SIF_{760} . The resultant SIF_{680}/SIF_{760} values showed a different response than the individual SIF values. The SIF_{680}/SIF_{760} ratio of barley and wheat slightly decreased between the 30th June and the 2nd July 2015. On the contrary, corn and rapeseed exhibit a slight increase in their SIF_{680}/SIF_{760} ratio within both acquisition dates. Both findings are illustrated in Figure 8h and 8g. Nevertheless, wheat showed both the minimum positive (0.0005) and the maximum (0.7652) SIF_{680}/SIF_{760} ratio value.

4.1.2 Vegetation indices

Structural indices

The three structural indices (SR, EVI and NDVI) showed equal responses within the four different crops (Figure 9d-f). All structural indices of barley, rapeseed and wheat decreased as a consequence of heat stress. On the contrary, the indices of corn increased during the heat wave. This is exactly the same behaviour that the SIF_{680} and SIF_{760} showed. Among the C_3 plants, barley and wheat showed a higher decrease in their SR values than rapeseed (Figure 9d). Barley exhibited a reduction of 18% and wheat a reduction of 46% between stressed and unstressed physiological status.

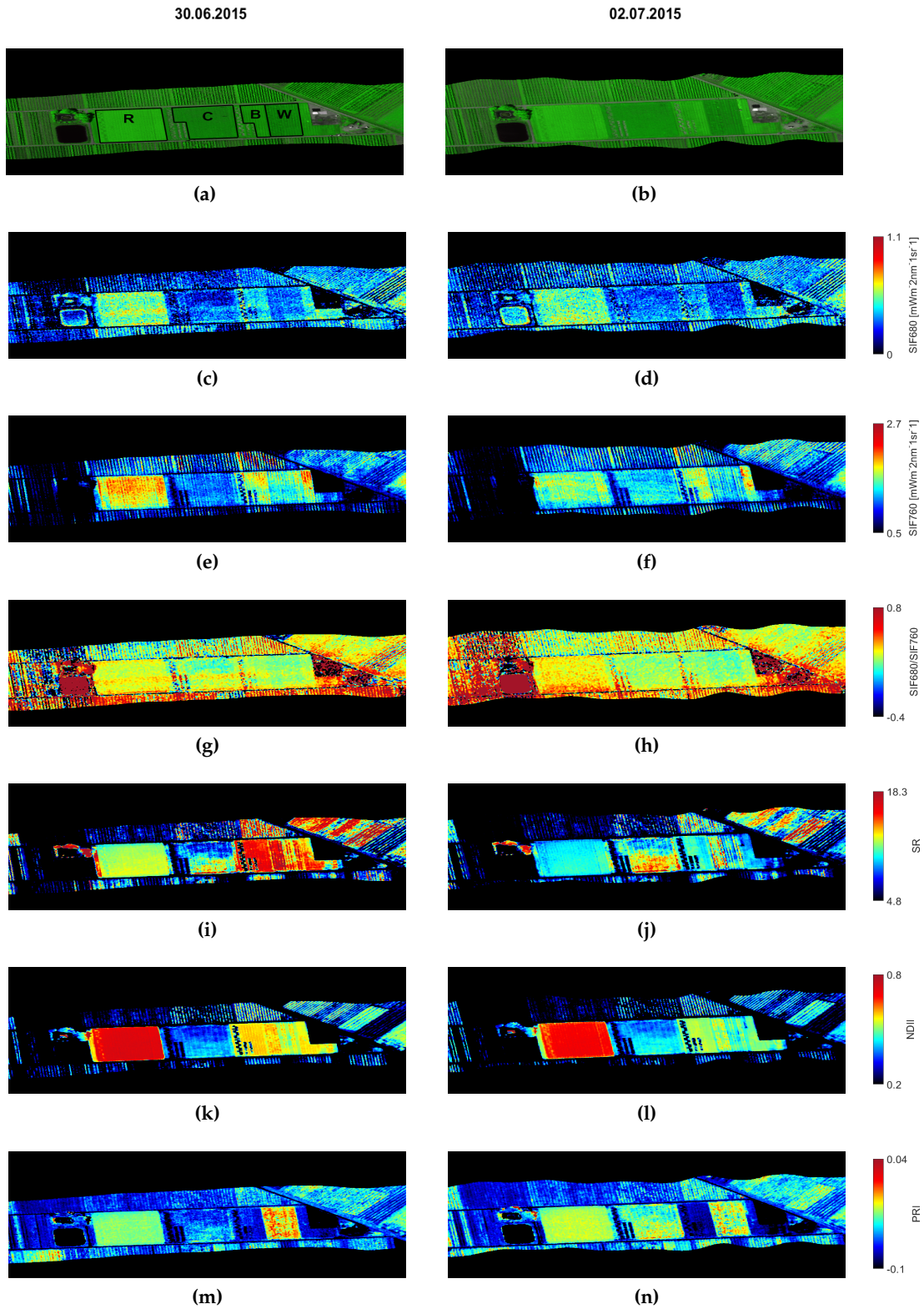


Figure 8: (a) and (b) are pseudo RGB composite images, with the reflectance at 697nm (red), 755nm (green) and 674nm (blue). The characters in (a) correspond to the barley (B), corn (C), rapeseed (R) and wheat (W) fields. SIF maps are illustrated in (c) to (h) and vegetation index maps in (i) to (n). Left maps were acquired on 30th June and right maps on 2nd July 2015.

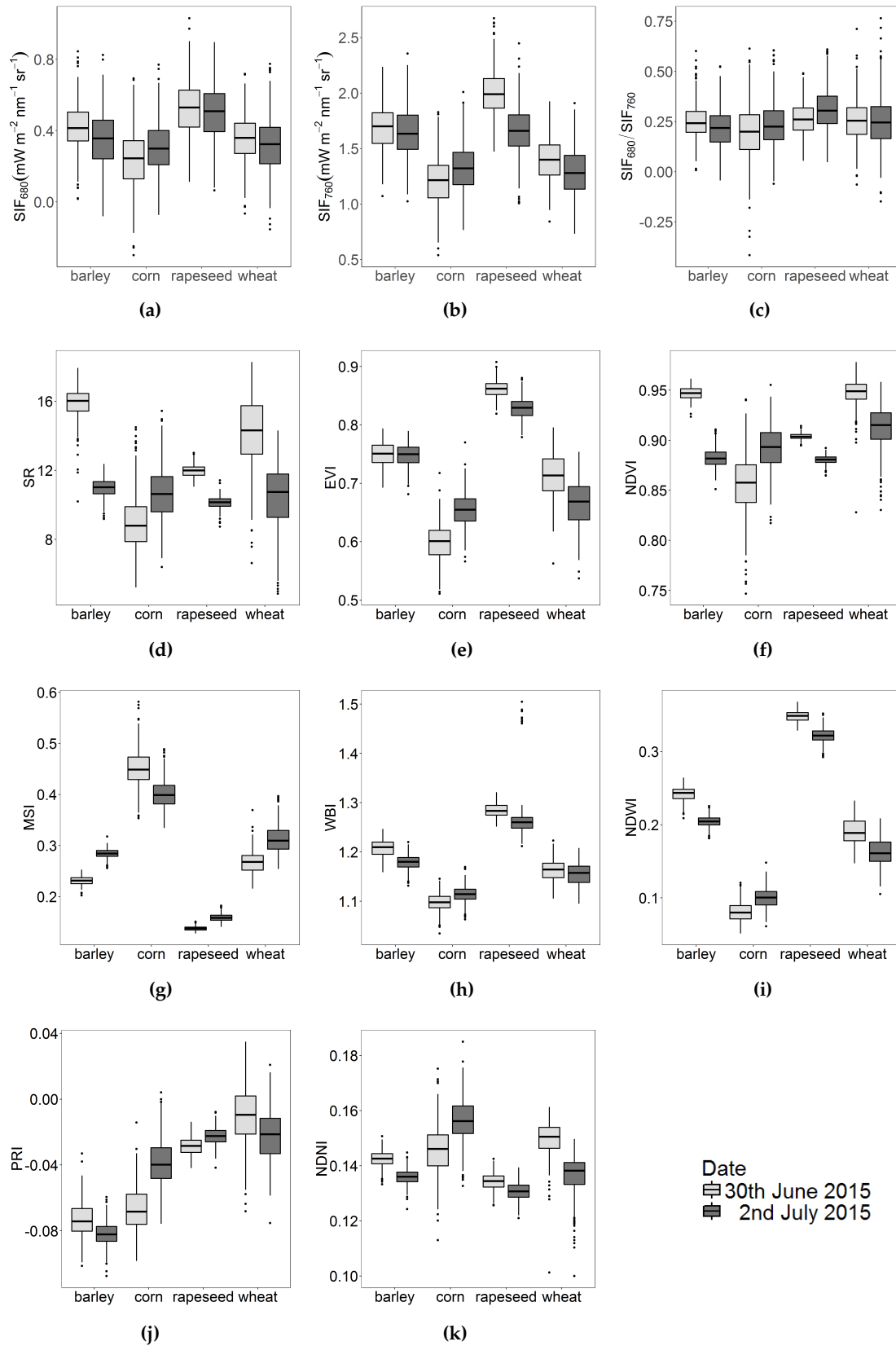


Figure 9: Boxplots of sun-induced chlorophyll fluorescence values and vegetation indices of corn, barley, rapeseed and wheat.

In addition, the lowest (4.8617, 2nd July 2015) and the highest (18.2725, 30th June 2015) SR values were measured in wheat. The decrease and increase of SR values during the heat wave are clearly illustrated in Figure 8i and 8j. The NDVI values range from 0.7468 to 0.9782, although corn had the lowest and wheat the highest value (Figure 9f). The maximum NDVI value (0.9782) is nearly 1 and indicates a saturation of the index at dense vegetation (Carlson and Ripley, 1997). However, the EVI is less sensitive to high biomass (Huete et al., 2002) and exhibited values between 0.5110 (corn) and 0.9077 (rapeseed), both measured on the 30th June 2015 (Figure 9e). Compared to the NDVI, all crops showed lower EVI values while the the highest index value was found in rapeseed and not in barley. Nevertheless, barley showed nearly no difference in its EVI values between both acquisition dates and as a result the smallest decrease (-12%) of all crops.

Water indices

The MSI, which is sensitive to leaf water content (Yilmaz et al., 2008) ranged from 0.1280 in rapeseed to 0.5815 in corn. Figure 9g shows, that only the MSI values of corn decreased during the heat wave. In contrast, the MSI values of the C₃ plants increased. The NDII, NDWI and the WBI, which are also sensitive to water in plant canopies (Gao, 1996; Hill, 2013; Peñuelas et al., 1993), typically decreased for C₃ plants and increased for corn. The values of the NDII ranged from 0.2313 to 0.7392, the values of the NDWI from 0.0514 to 0.3681 and the values of the WBI from 1.0347 to 1.5047. In summary, all water indices revealed a decreasing plant water content (Gao, 1996; Hill, 2013; Hunt and Rock, 1989; Peñuelas et al., 1993). The water indices are visualized in Figure Figure 9g-i, whereby the NDII is not illustrated because it looks similar like the NDWI boxplot (see appendix for visualization). Nevertheless, the NDII was visualized in Figure 8k and 8l and shows the different water responses of the crops. It is clearly visible, that the water content of barley and wheat decreased during the heat wave.

Functional indices

The measured PRI values ranged from 0.0349 (on 30th June 2015) to -0.1074 (on 2nd July 2015). Corn and rapeseed both showed an increase in PRI values between the 30th June 2015 and the 2nd July 2015. In addition, Figure 9j reveals that the averaged PRI values of corn and rapeseed increased, approaching zero. Inversely, the PRI values of barley and wheat decreased. Corn exhibited (in contrast to the C₃ crops) the biggest difference in its PRI values between both acquisition dates. These findings are also visible in the PRI maps of Figure 8m and 8n.

The nitrogen status of the plants was measured by the NDNI and is illustrated in Figure 9k. The NDNI showed values between 0.1 and 0.185. Obviously, the NDNI of the C₃ plants decreased during the heat wave, whereas the NDNI of corn increased.

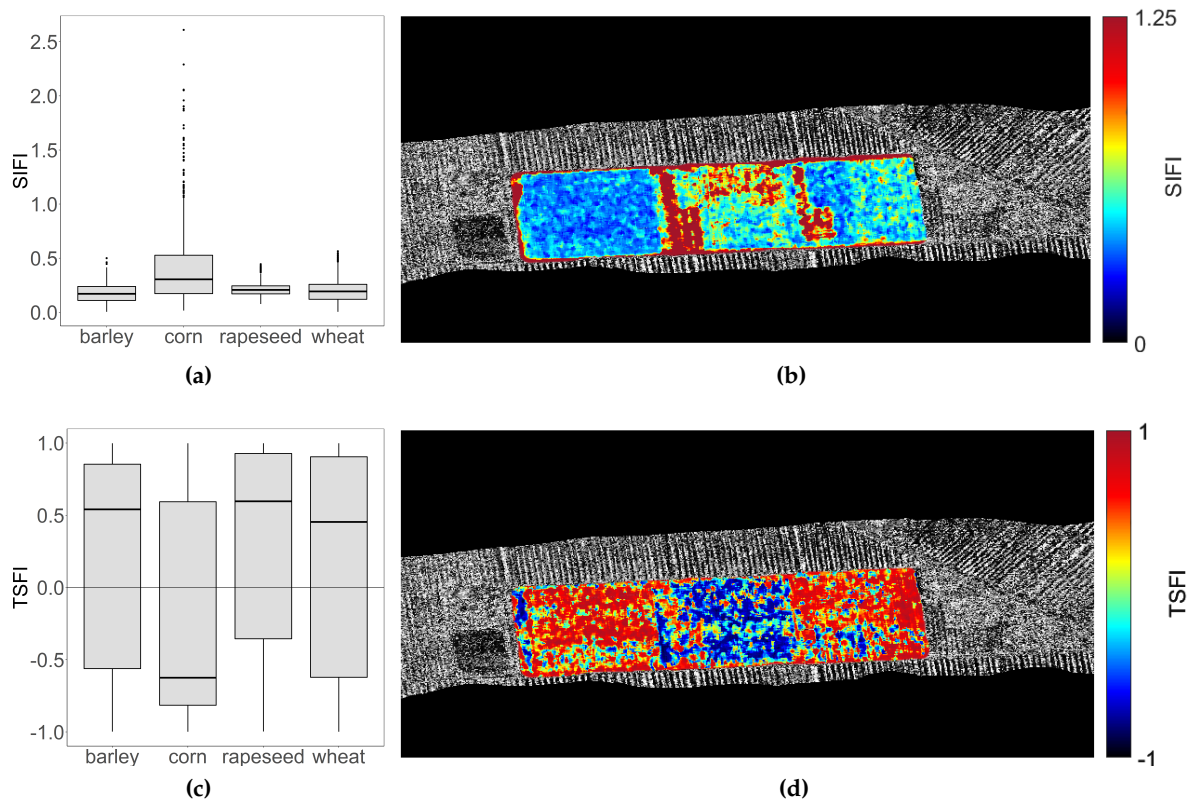


Figure 10: Stress Intensity Fluorescence Index (SIFI) and Temperature Stress Fluorescence Index (TSFI) of barley, corn, rapeseed and wheat during the heat wave in summer 2015. Boxplots of the SIFI and TSFI are illustrated in (a) and (c), whereby the maps are illustrated in (b) and (d).

4.1.3 Stress Fluorescence Index

Figure 10 shows the Stress Intensity Fluorescence Index (Equation 18) and the Temperature Stress Fluorescence Index (Equation 21) of all plants. Due to the fact, that the data had a lot of noise, the data was filtered by a 5x5 median filter, reducing the amount of outliers. The boxplots of Figure 10a and Figure 10c illustrate the different responses of the four crop types. The C_3 crops had lower SIFI and positive TSFI values, whereby corn showed higher SIFI and negative TSFI values. Consequently, corn exhibited the highest stress intensity but another stress response than the C_3 plants. However, all crops showed at least a small stress response during the heat wave, as all median values were unequal zero. The stress responses of the four crops are visualized in the SIFI and TSFI maps in Figure 10b and 10d. It is clearly visible that corn showed a more distinct stress response than barley, rapeseed and wheat.

4.1.4 Pearson correlation between sun-induced chlorophyll fluorescence and vegetation indices

The Pearson correlation coefficients were calculated to compare sun-induced chlorophyll fluorescence and vegetation indices. Table 3 shows an overview of the correlation coefficients of barley,

Plant	SIF	SR	NDVI	EVI	PRI	NDNI	WBI	NDWI	MSI	NDII
Barley	680	0,051	-0,020	-0,009	0,021	-0,092	0,014	0,088	-0,040	0,028
	760	0,043	-0,129	-0,054	-0,009	-0,031	-0,035	-0,062	0,074	-0,070
	680/760	0,034	0,037	0,023	0,028	-0,063	0,020	0,106	-0,067	0,057
	SIFI	0,049	-0,034	0,007	0,078	0,007	0,017	0,022	-0,007	0,018
Corn	680	0,235	0,029	0,009	-0,025	0,032	-0,006	-0,022	-0,010	0,006
	760	0,119	-0,052	-0,040	-0,104	-0,030	-0,040	-0,085	0,054	-0,076
	680/760	0,204	0,058	0,023	0,001	0,041	0,012	0,011	-0,037	0,040
	SIFI	0,112	0,063	0,016	0,001	0,020	0,048	0,061	-0,064	0,069
Rapeseed	680	0,034	-0,062	-0,007	-0,076	0,005	-0,059	-0,064	0,087	-0,084
	760	0,050	0,005	0,021	0,043	0,012	0,001	-0,028	0,002	-0,014
	680/760	0,006	-0,049	-0,008	-0,099	0,001	-0,054	-0,052	0,084	-0,076
	SIFI	-0,094	-0,035	-0,006	-0,034	-0,016	-0,058	-0,032	0,061	-0,063
Wheat	680	0,274	0,039	0,189	-0,026	0,144	-0,071	-0,015	-0,029	0,034
	760	0,494	0,143	0,293	0,038	0,275	0,002	0,067	-0,199	0,192
	680/760	0,094	0,010	0,076	-0,022	0,055	-0,065	-0,028	0,031	-0,024
	SIFI	-0,425	-0,066	-0,239	-0,015	-0,189	0,005	-0,059	0,150	-0,149
All crops	680	0,287	0,219	0,173	0,145	0,185	0,087	0,190	-0,208	0,206
	760	0,263	0,192	0,351	0,133	0,239	0,153	0,250	-0,234	0,231
	680/760	0,199	0,158	0,056	0,104	0,111	0,036	0,105	-0,131	0,131
	SIFI	-0,028	-0,018	-0,058	-0,005	-0,003	-0,036	-0,046	0,032	-0,035

Table 3: Pearson correlation coefficient between the sun-induced chlorophyll fluorescence and the vegetation indices.

corn, rapeseed and wheat between the SIF_{680} , SIF_{760} , SIF_{680}/SIF_{760} , SIFI and the vegetation indices. To compare the sun-induced chlorophyll fluorescence, SIFI and vegetation indices, the values of the 30th June 2015 were subtracted from the values of the 2nd July 2015. The resultant differences were compared by means of a Pearson correlation. As Table 3 indicates, the correlation most frequently lay between 0 and ± 0.1 , indicating a very small correlation between sun-induced chlorophyll fluorescence and vegetation indices. As an exception, corn showed higher correlation coefficients between all SIFI and SR values (correlation lay between 11 to 24%). The highest correlation coefficient was revealed for wheat between SIF_{760} and SR ($r = 0.49$). Considering all crops together, the correlation was most frequently higher than 10% but smaller than 35%. Consequently, the Pearson correlation (Table 3) indicates high added values of SIF compared to vegetation indices.

4.2 Light stress

The light stress experiment is visualized in Figure Figure 11a-d. SIF_{680} and SIF_{760} maps (Figure 11a and b) clearly illustrate that the last two meters, where the sugar beet was under high light stress, is coloured differently than the rest of the sugar beet field. The last two meters are coloured yellowish to reddish whereby the rest of the sugar beet field is coloured in blue and green shades. This finding

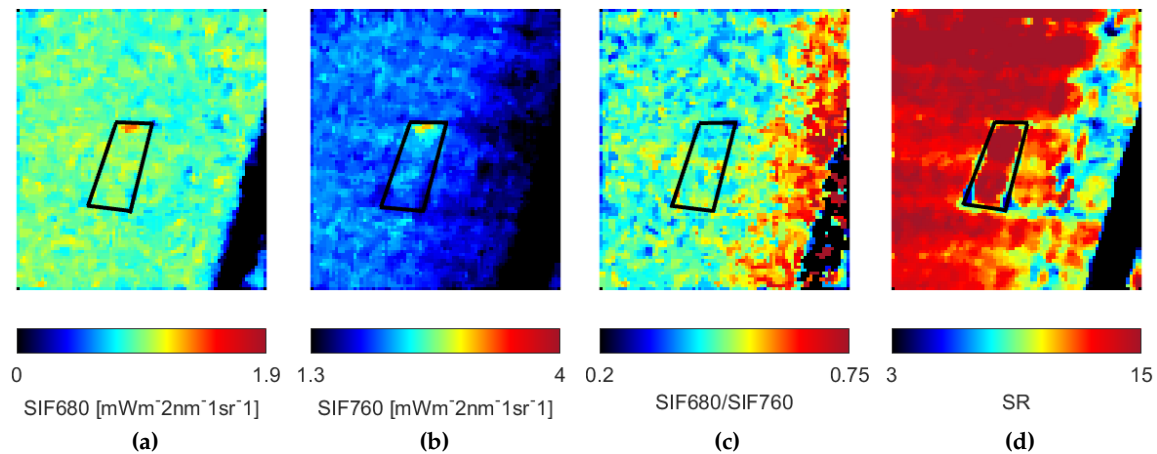


Figure 11: Sun-induced chlorophyll fluorescence and SR maps of the light stress experiment. The black rectangle illustrates the net above the sugar beet. The last two meters, where the net was removed immediately before the aircraft passed, are inside at the top of the rectangle. (a) represents SIF_{680} , (b) SIF_{760} , (c) SIF_{680}/SIF_{760} and (d) the SR.

indicates higher SIF_{680} and SIF_{760} values within light stressed sugar beet. The SIF_{680}/SIF_{760} ratio decreased slightly with increasing light stress. Additionally, the SR in Figure 11d shows high values over the whole sugar beet field, with only small variations within the SR values.

4.2.1 Sun-induced chlorophyll fluorescence and simple ratio

In the course of the light stress experiment sugar beet exhibited SIF_{680} values between -0.2687 and $1.8454 \text{mWm}^{-2}\text{nm}^{-1}\text{sr}^{-1}$ and SIF_{760} values between 1.3396 and $3.9644 \text{mWm}^{-2}\text{nm}^{-1}\text{sr}^{-1}$. Ignoring the negative values, the lowest SIF_{680} value of the light stress experiment is $0.4844 \text{mWm}^{-2}\text{nm}^{-1}\text{sr}^{-1}$. Irrespective of the light stress condition, SIF_{680} values were lower than SIF_{760} values. Both, the lowest SIF_{680} and SIF_{760} values, were measured half an hour after the net removal and the highest values were measured immediately after the net removal. It is clearly visible in Figure 12a and 12b (as well as Figure 11a and 11b) that sun-induced chlorophyll fluorescence values at both spectral regions increased with increasing light stress. SIF_{760} showed a higher increase than SIF_{680} . The ratio between SIF_{680} and SIF_{760} revealed only small changes during the experiment (Figure 12c) and ranged from -0.2006 to 0.7438 .

The SR exhibited values between 3.5472 and 13.1246 . Figure 12d shows the SR over time, indicating an increase of the SR until 10 minutes before the aircraft passed. Afterwards the SR decreased. Furthermore, the SR decreased at the exact same point where the SIF_{680} decreased and the SIF_{760} increased.

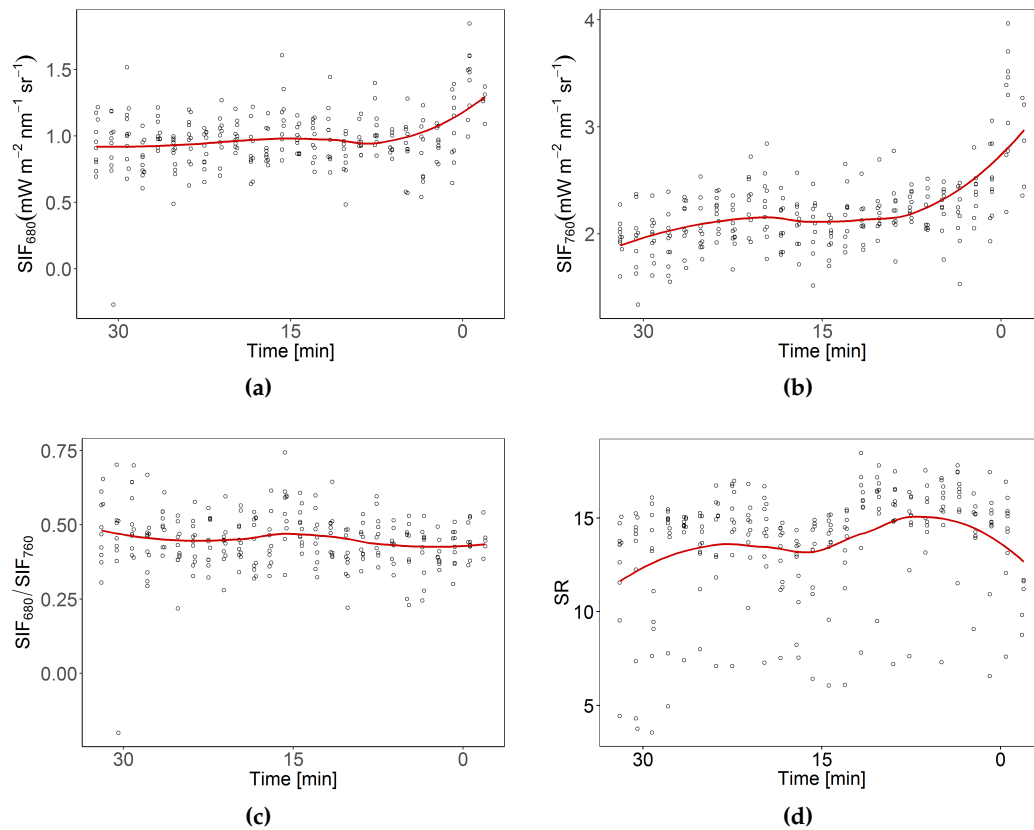


Figure 12: Scatterplots of (a) SIF_{680} , (b) SIF_{760} , (c) SIF_{680}/SIF_{760} and (d) SR values. The red line is a locally fitted polynomial regression line. The net was rolled up slowly and continuously 30 minutes before the aircraft passed and the last two meters of the net were removed only seconds before the overpass at Time 0.

4.2.2 Light Stressed Fluorescence Index

The SIFI was calculated according to Equation 18 and the Light Stress Fluorescence Index (LSFI) according to Equation 20. Both the scatterplots in Figure 13a and 13c and the maps in Figure 13b and 13c show an increase of the SIFI and LSFI values with increasing light stress. The LSFI values increased earlier than the SIFI values, which increased only a few minutes before the aircraft passed. The majority of the calculated LSFI values lay between 0 and 1, indicating a light stress response of sugar beet.

4.2.3 Pearson correlation

The Pearson correlation coefficients showed almost no correlation between the SR and the SIF_{680} (0.0538), SIF_{760} (0.1646), SIF_{680}/SIF_{760} (-0.0552) and SIFI (-0.0749). Consequently, the highest correlation was found between the SR and SIF_{760} , whereas the lowest correlation was found between the SR and SIF_{680} . This result revealed a high added value of the sun-induced chlorophyll fluorescence within the light stress experiment.

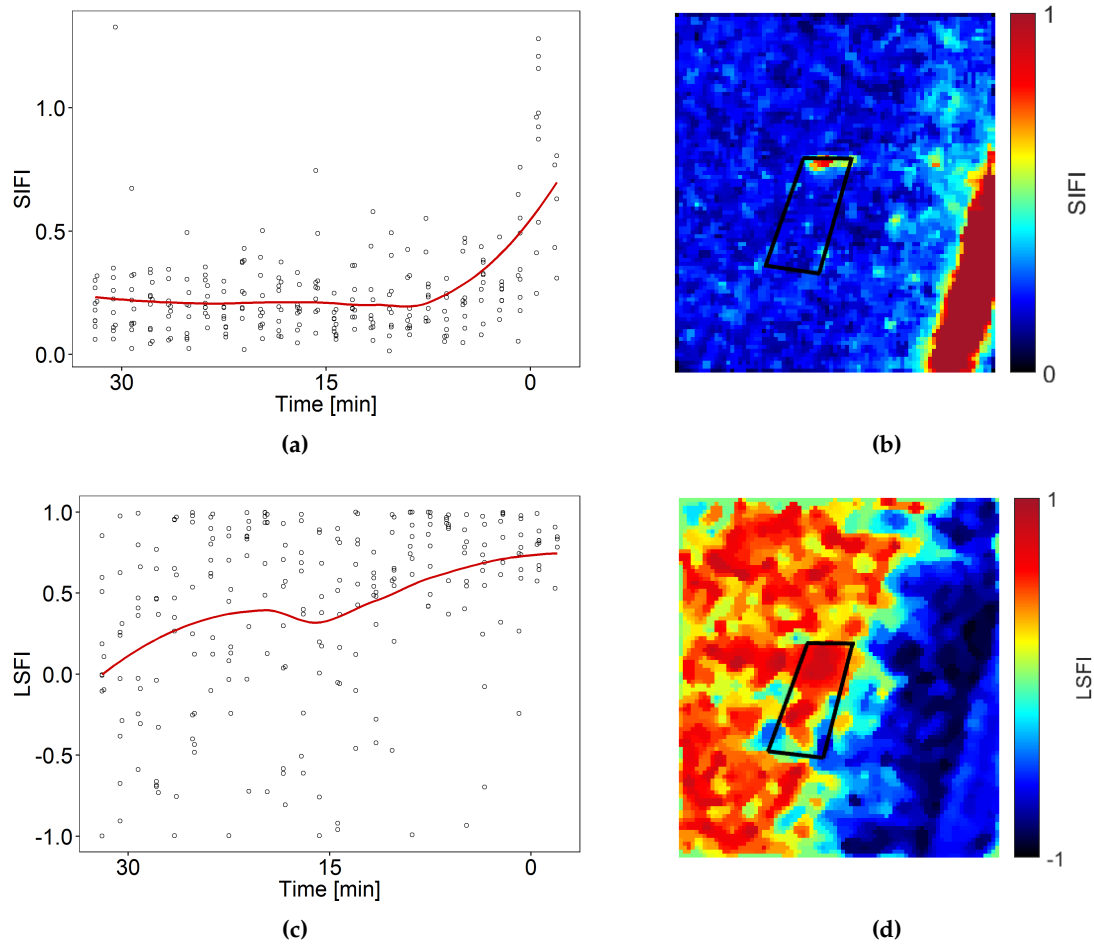


Figure 13: Stress intensity fluorescence index (SIFI) and light stress fluorescence index (LSFI) of sugar beet. (a) and (c) show the scatterplots of the SIFI and LSFI values with a locally fitted polynomial regression line in red. The net was removed immediately at time 0 when the aircraft passed. (b) and (d) illustrate the SIFI and LSFI maps with a black rectangle indicating the position of the net.

4.3 Water stress

Figure 14a-h illustrate the SIF_{680} values of the water stress experiment. The visualization points out the difference between water unstressed and stressed sugar beet, as well as the daily course of sun-induced chlorophyll fluorescence values.

4.3.1 Sun-induced chlorophyll fluorescence and simple ratio

Figure 15a, 15b, 15e and 15f depict the SIF_{680} and SIF_{760} values of stressed and unstressed sugar beet during the day. Excluding negative SIF_{680} values, the lowest SIF_{680} value was 0.0052 and the highest $1.6644 \text{mWm}^{-2}\text{nm}^{-1}\text{sr}^{-1}$. SIF_{760} values ranged from 0.2549 to $3.2738 \text{mWm}^{-2}\text{nm}^{-1}\text{sr}^{-1}$. It is clearly visible in Figure 15 that SIF_{760} exhibited, as opposed to SIF_{680} , a stronger decrease between unstressed and stressed sugar beet. Both, SIF_{680} and SIF_{760} showed the highest values at solar noon coinciding with high solar radiation. Consequently, SIF values were lower before and after solar noon. Unstressed sugar beet revealed, in contrast to stressed sugar beet, higher SIF_{680} and SIF_{760} values. As an exception, stressed sugar beet on field 1 showed higher SIF_{680} values than unstressed sugar beet on the same field at solar noon (Figure 15a). In addition, the boxplots of SIF_{680} and SIF_{760} illustrate the daily course of the sun-induced chlorophyll values, independent of the physiological plant status.

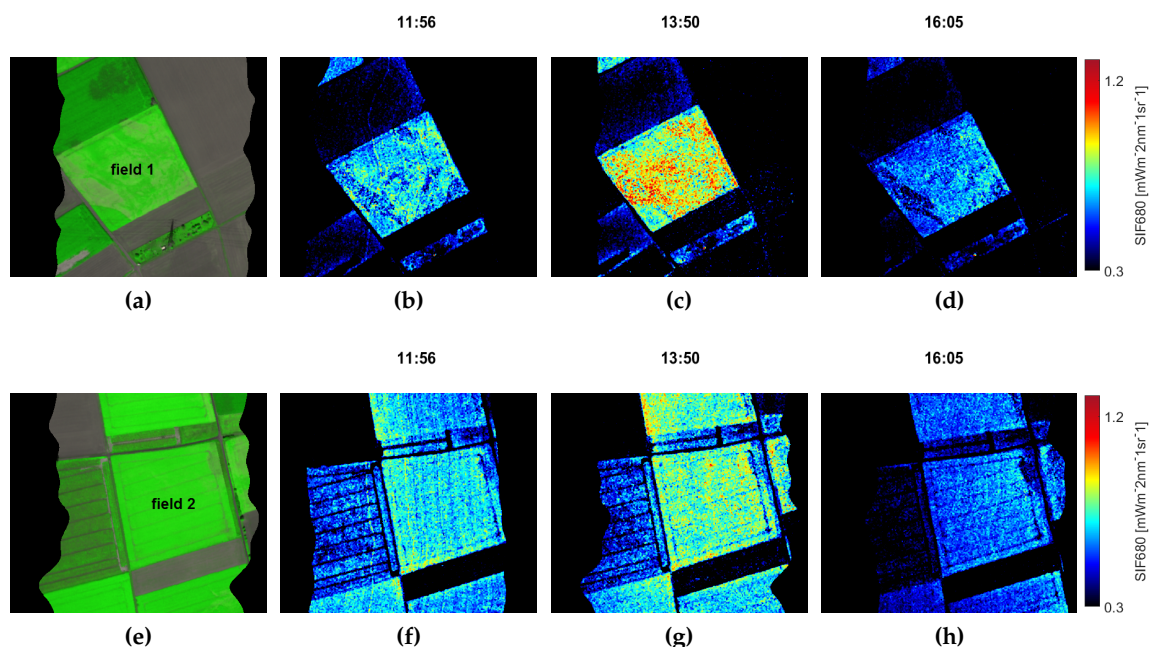


Figure 14: Sun-induced chlorophyll fluorescence maps at 680nm before (11:56), at (13:50) and after (16:05) solar noon (local time) of sugar beet field 1 and field 2 on 23rd August, 2012. Sugar beet field 1 is illustrated in (a) to (d) and sugar beet field 2 in (e) to (h). (a) and (e) represent the pseudo-RGB map of field 1 respectively field 2 with the reflectance at 697nm (red), 755nm (green) and 674nm(blue)).

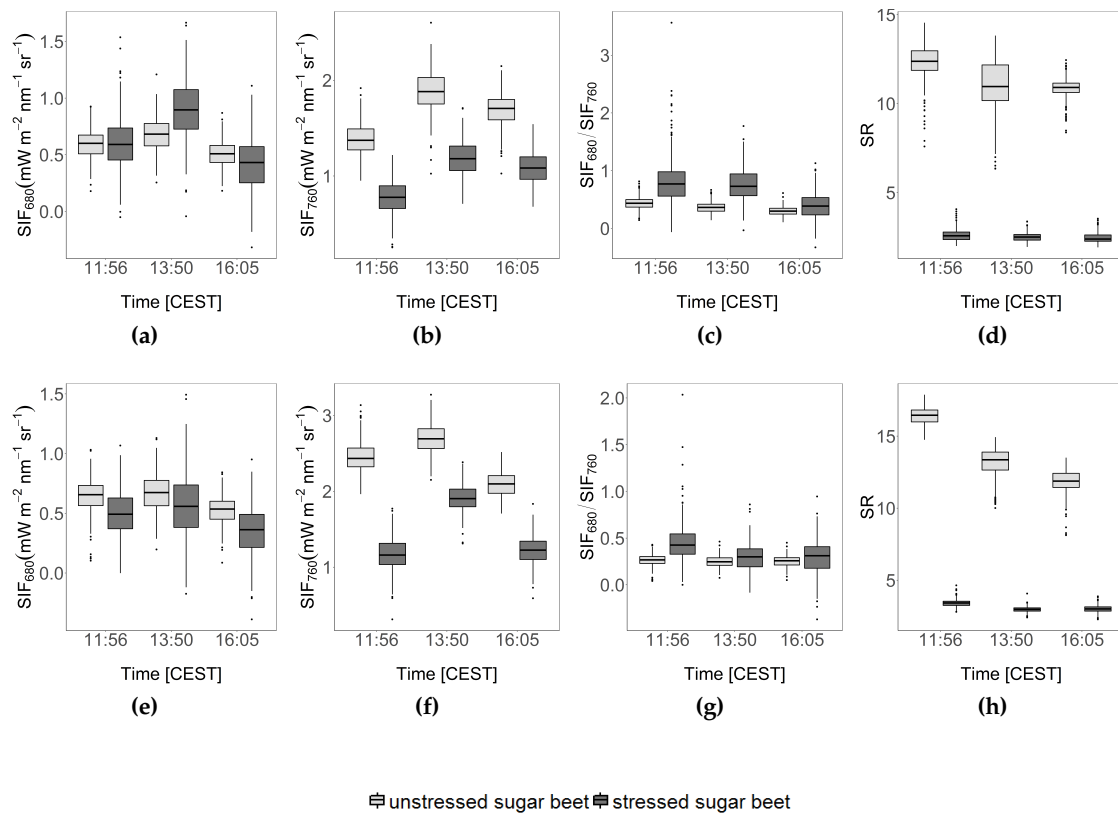


Figure 15: Boxplots of SIF_{680} , SIF_{760} , SIF_{680}/SIF_{760} and the SR of sugar beet at the three acquisition times (11:56, 13:50 and 16:05) on 23rd August 2012. Figure (a) to (d) belong to sugar beet on field 1 and Figure (e) to (h) to sugar beet on field 2.

The SIF_{680}/SIF_{760} ratio is illustrated in Figure 15c and 15g and ranged from -0.3701 to 3.5621. In contrast to SIF_{680} , SIF_{760} and SR, SIF_{680}/SIF_{760} values are higher in stressed than in unstressed sugar beet. Furthermore, stressed and unstressed sugar beet on field 1 revealed a decrease in their SIF_{680}/SIF_{760} values during the course of the day. This finding is not consistent with sugar beet on field 2. Unstressed sugar beet on field 2 showed almost no visible change during the course of the day and stressed sugar beet on field 2 exhibited the lowest SIF_{680}/SIF_{760} value at solar noon (Figure 15g).

The SR ranged from 1.9258 to 17.8724. The highest SR value was measured before solar noon in stressed sugar beet on field 1 and the lowest at solar noon in stressed sugar beet on field 2. Considering the three acquisition times, the SR decreased between unstressed and stressed sugar beet as well as during the course of the day (Figure 15c). Figure 15d and h illustrate that SR decreased considerably more than the SIF values. The average decrease of the SR between unstressed and stressed sugar beet is 77.5%.

4.3.2 Water Stress Fluorescence Index

Diurnal variations are not only exhibited in SIF and SR values but also in the SIFI and Water Stress Fluorescence Index (WSFI). The SIFI was calculated according to Equation 18 and the WSFI according to Equation 22. The SIFI and WSFI of both fields before, after and at solar noon are illustrated as boxplots in Figure 16 and as maps in Figure 17. The boxplots show that unstressed sugar beet had values around zero, whereas stressed sugar beet had higher values. Additionally, the boxplots illustrate unequal responses of stressed sugar beet on field 1 and field 2. Stressed sugar beet on field 2 (Figure 16c) exhibited lowest SIFI values at solar noon, whereby the lowest SIFI values of sugar beet on field 1 occurred after solar noon. The lowest WSFI values at solar noon had sugar beet on field 1 (Figure 16b). Median WSFI values of stressed sugar beet on field 2 slightly increased over the course of the day. The WSFI of stressed sugar beet on field 1 showed the opposite reaction to unstressed sugar beet on field 1. Nevertheless, the majority of the WSFI values of stressed sugar beet lay between 0 and 1, which refer to water stress responses. Both maps of Figure 17 illustrate, similar to the boxplots of Figure 16, the diurnal variation of the SIFI and the WSFI in sugar beet. Furthermore, the difference between stressed and unstressed sugar beet is clearly visible.

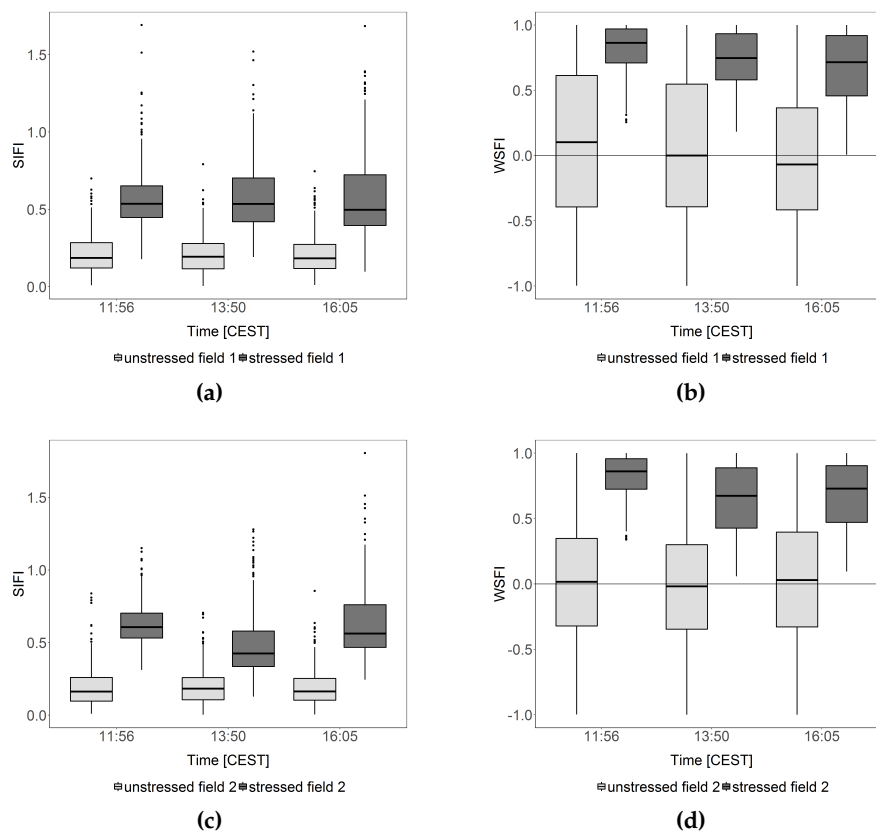


Figure 16: SIFI boxplots of sugar beet field 1 (a) and sugar beet field 2 (c) and WSFI boxplots of sugar beet field 1 (b) and sugar beet field 2 (d) before (11:56), after (16:05) and at solar noon (13:50) on 23rd August 2012.

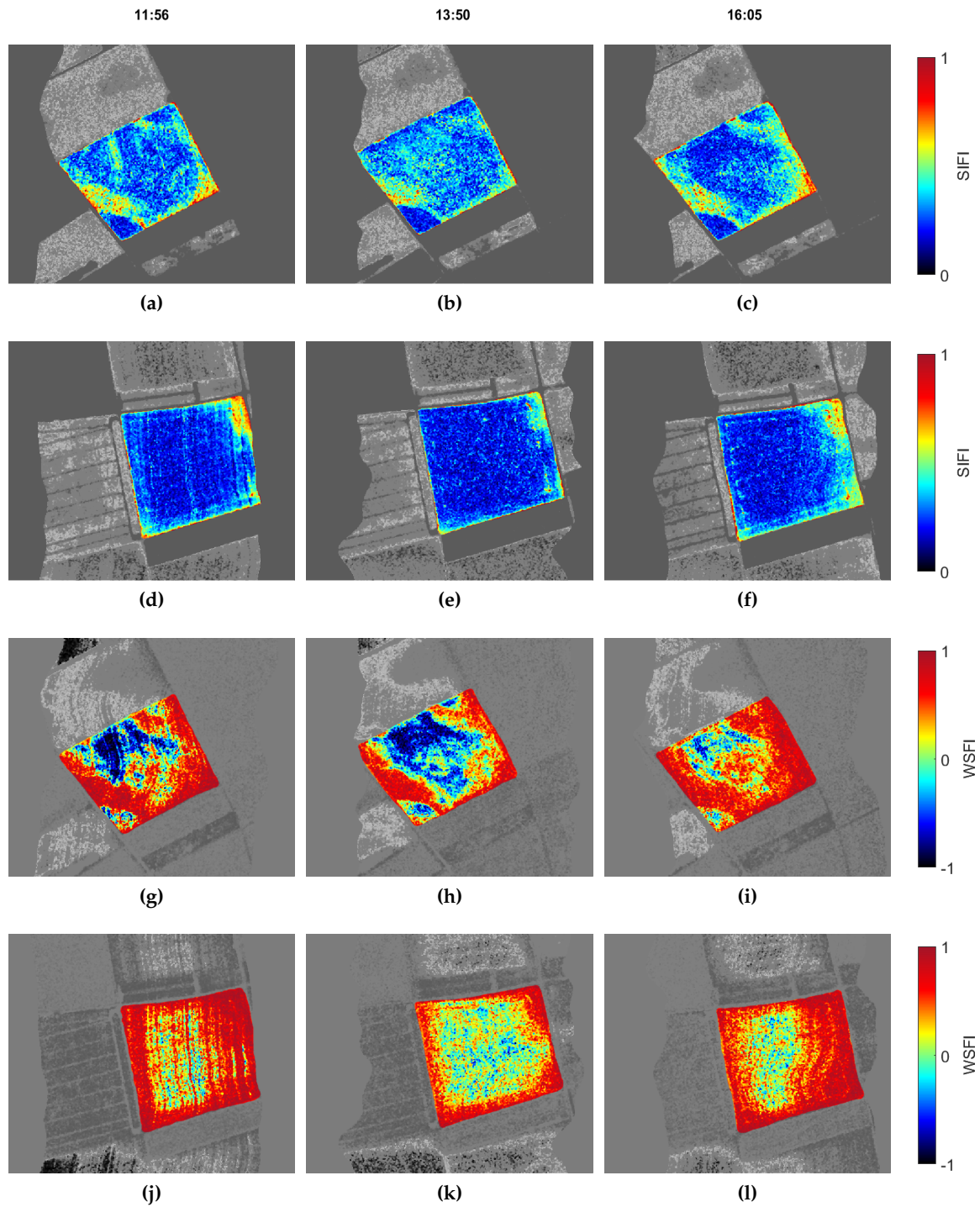


Figure 17: SIFI and WSFI maps of sugar beet field 1 and sugar beet field 2 before (11:56), after (16:05) and at solar noon (13:50) on 23rd August 2012. Sugar beet field 1 is depicted in (a) to (c) and (g) to (i), whereby sugar beet field 2 in (d) to (f) and (j) to (l).

4.3.3 Pearson correlation between sun-induced chlorophyll fluorescence and simple ratio

Sugar beet showed higher correlation coefficients between SIF and SR values during the water stress experiment in contrast to sugar beet during the light stress experiment. The SR revealed a correlation coefficient of 0.1255 with SIF_{680} , 0.7357 with SIF_{760} , -0.3614 with SIF_{680}/SIF_{760} and -0.6910 with the SIFI. Consequently, the highest added value (87.45%) was achieved with SIF_{680} and the lowest with SIFI (30.89%).

4.4 Bi-dimensional parameter space of vegetation stress

The bi-dimensional parameter space, defined by the SIF_{680} and SIF_{760} values is illustrated in Figure 18. The results of the meta-analysis from Mohammed et al. (2014) with nitrogen (N_{lit}), temperature (T_{lit}) and water (W_{lit}) stress are illustrated in grey. The coloured boxes and points were calculated with the data from the light (orange), heat (red) and the water (blue) experiment. All boxes are defined by the standard deviations of the stressed to unstressed SIF_{680} and SIF_{760} values and the normalized mean values are labelled as L_{exp} , T_{exp} and W_{exp} respectively. Since the SIF_{680} values of the heat experiment had a high noise, the standard deviation was exceptionally large. As a consequence, the heat stress data was smoothed by a 5x5 median filter. Thus, the boxes of the

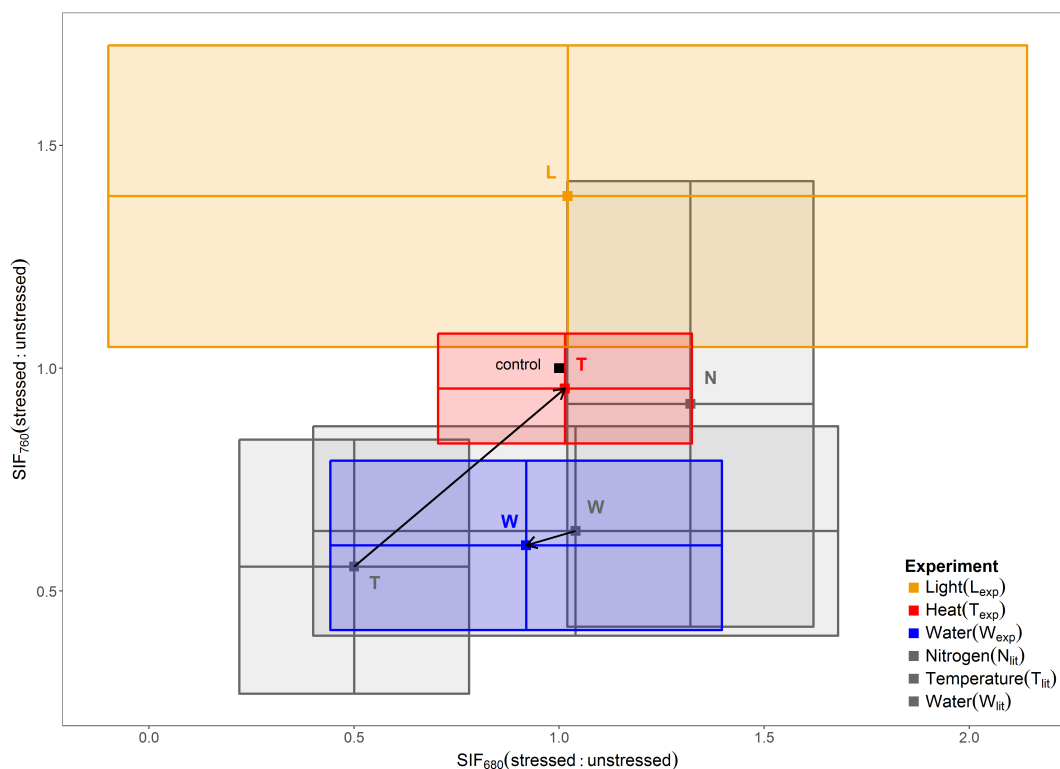


Figure 18: Representation of the light (yellow), heat (red) and water (blue) stress experiment in a bi-dimensional parameter space defined by SIF_{680} and SIF_{760} values.

heat stress experiment fit into the parameter space. The differences between the mean values of Mohammed et al. (2014) and the mean values of the heat and water stress experiment are indicated with black arrows (Figure 18). It is clearly visible that the experimental findings of the heat stress experiment do not match with the findings of Mohammed et al. (2014), but the findings of the water stress experiment coincide.

The heat stress experiment had a standardized SIF_{680} mean value of 1.0138 and a SIF_{760} mean value of 0.9546. These standardized mean values are approximately twice as large the values of Mohammed et al. (2014) and nearly 1, indicating a minor increase in stress levels. In addition, this small deviation of the heat stress mean value to the control values is also visible in the low SIFI values of the heat stress experiment (Section 4.1.3). The water experiment showed a standardized SIF_{680} mean value of 0.9603 and a standardized SIF_{760} mean value of 0.6065, which are the lowest mean values within the three stress experiments. In contrast, the light stress experiment displayed the highest standardized mean values. It exhibited a SIF_{680} mean value of 1.0208 and a SIF_{760} mean value of 1.3861. Consequently, the light stress experiment is located in the upper part of the parameter space. Furthermore, it showed, similar to the heat stress experiment, high SIF_{680} standard deviations, displayed as a large orange box in Figure 11.

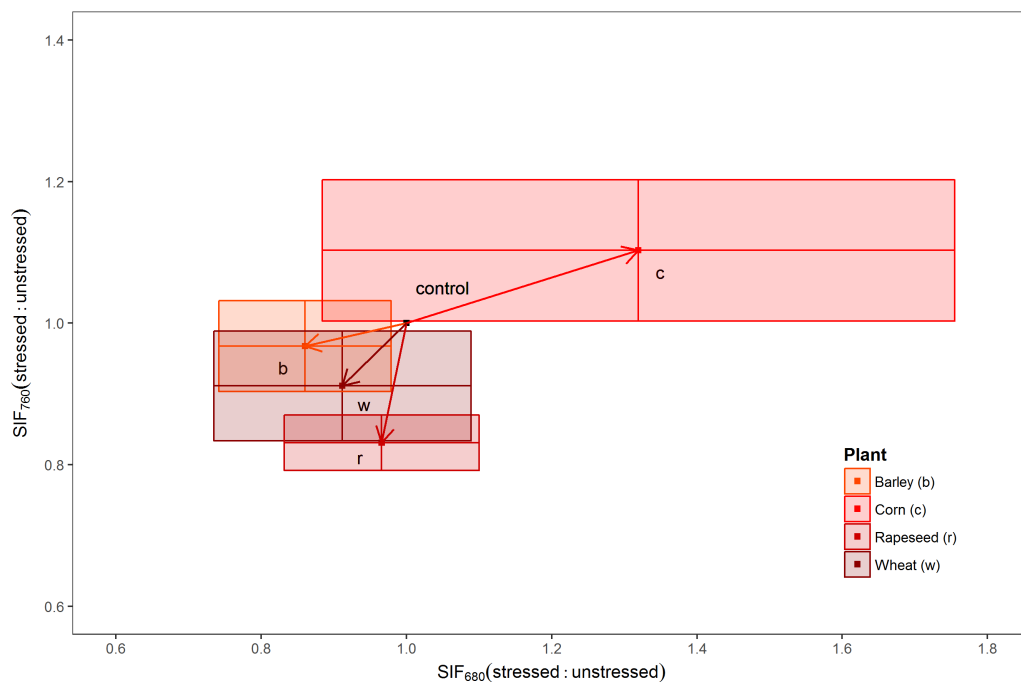


Figure 19: Representation of the heat stress experiment in the bi-dimensional parameter space defined by SIF_{680} and SIF_{760} values. The heat stress data was classified by the four different plant species. The four arrows indicate SIFI values of each crop.

4.4.1 Heat stress

Figure 19 clearly illustrates that the C₃ crops showed a slight heat stress response because they are located in the lower part of the bi-dimensional parameter space and their SIFI arrows are greater than zero but short. Furthermore, it is visible that corn showed no heat stress reaction because the parameter box of corn is not located in the lower part of the bi-dimensional parameter space. In fact, corn showed another stress response since corn exhibited the largest SIFI values (Figure 10) within the heat stress experiment. These findings were already illustrated in Figure 10c and d. Additionally, Figure 19 exhibits, that corn has the highest standard deviation, manifesting highest noise in SIF₆₈₀ values.

4.4.2 Light stress

The light stress experiment was split up in three different acquisition times and illustrated in the bi-dimensional parameter space in Figure 20. The net over the sugar beet field was removed only seconds before the aircraft passed at t_0 . As a consequence, Figure 20 highlights the increase of light stress with acquisition time: the more stressed the higher the SIF₆₈₀ and SIF₇₆₀ values of sugar beet. Additionally, the arrows illustrate the increase of the SIFI and LSFI with increasing light stress as illustrated in Figure 13. The high standard deviation in SIF₆₈₀ of the light stress box in Figure 18 originates from the SIF₆₈₀ values of stressed sugar beet at t_0 .

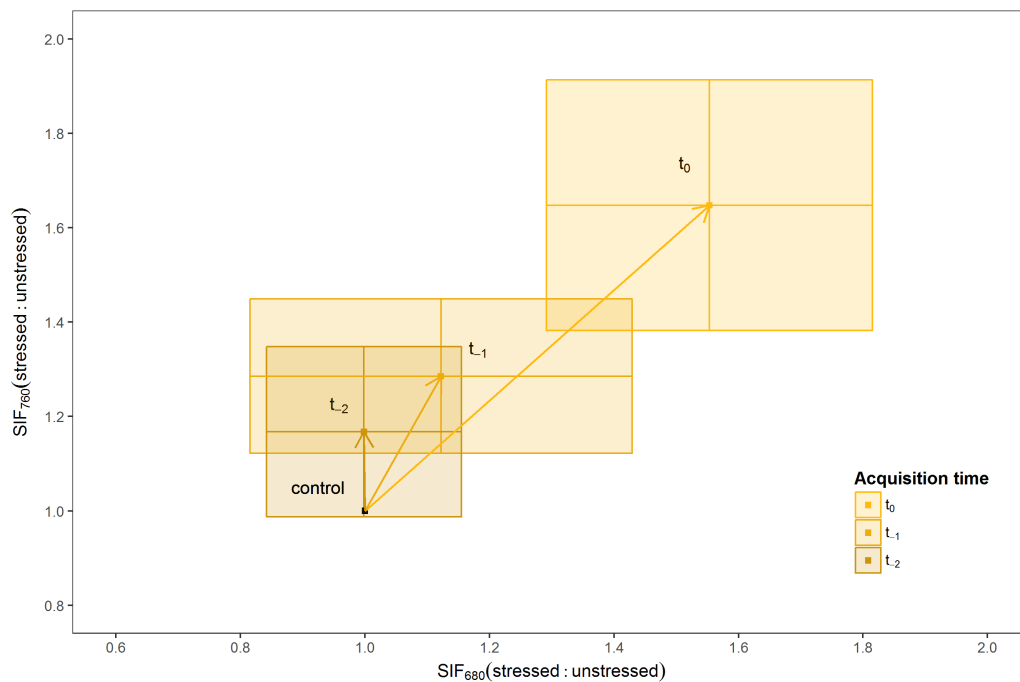


Figure 20: Light stress representation in the bi-dimensional parameter space defined by SIF₆₈₀ and SIF₇₆₀ values. The light experiment data was classified by three different acquisition times. Arrows indicate SIFI values of sugar beet at the corresponding acquisition time.

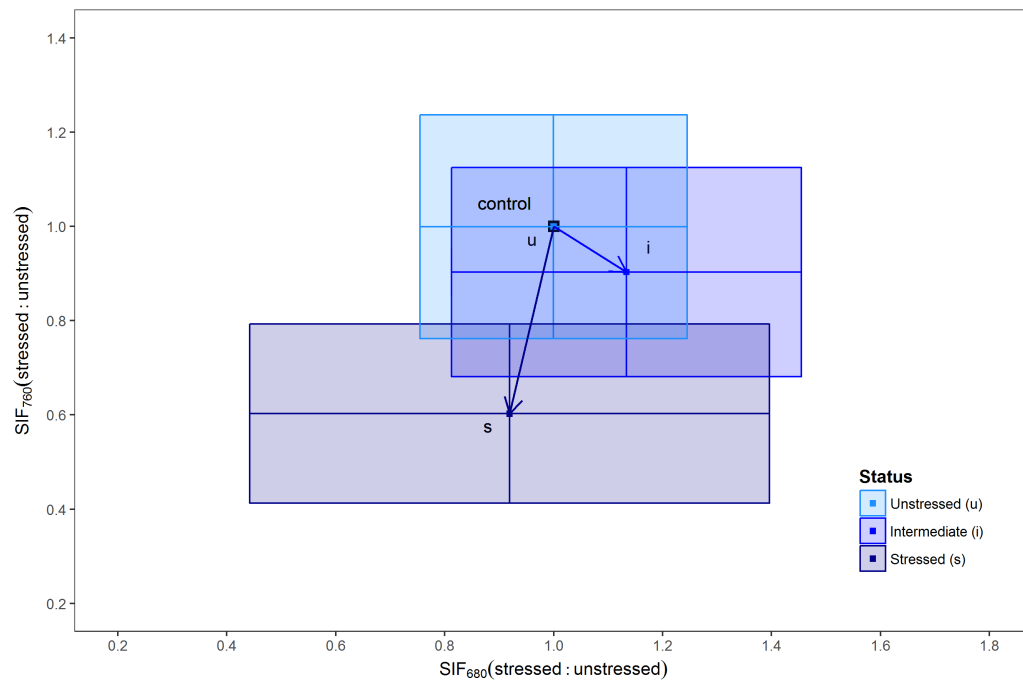


Figure 21: Representation of the water stress experiment in the bi-dimensional parameter space defined by SIF_{680} and SIF_{760} values. The water stress experiment was subdivided into stressed, intermediate stressed and unstressed sugar beet. The corresponding SIFI values are indicated by arrows.

4.4.3 Water stress

Figure 21 shows the water stress experiment with sugar beet. In addition to stressed and unstressed, an intermediate stressed sugar beet part on field 1 and field 2 was selected in a ROI and illustrated in the bi-dimensional parameter space. It is clearly visible that SIF_{760} values decreased in contrast to SIFI and WSFI values, which increased with increasing water stress. Figure 21 shows, similar to Figure 16, that unstressed sugar beet is not stressed at all and perfectly matches with the control point.

5 Discussion

5.1 Experimental settings

All experiments were characterised by unique experimental setups as they were conducted with different plant species and environmental stressors on different spatio-temporal scales. The heat stress experiment exhibited a time scale of days and was carried out without a control group as all plants were subjected to heat stress. Consequently, the heat stress experiment was the only experiment which allowed to monitor stress responses of the same plants at identical location. In contrast to the heat stress experiment, the light stress experiment was a shorter time period of only a couple of minutes and within a much smaller spatial extent. The experiment aimed at examining how to examine how plants respond to sunlight after they were exposed to a short period of reduced light intensities. As the plants were not susceptible to exceptional light intensities, it was thus much less a light stress experiment but rather a light response experiment to naturally varying light intensities. The third experiment, specifically the water stress experiment was carried out at two different time scales. The plants were exposed to drought over a time scale of days and weeks, while the acquisitions took place within several hours on one day under different solar irradiations. In particular, the difference between drought stressed and unstressed plants and how they respond to the daily course of sunlight was monitored.

5.2 Reliability of sun-induced chlorophyll fluorescence

Even though the data was subject to precise atmospheric, sensor and transmittance corrections, it can have small biases. These small biases occur as the emitted and reflected radiance fluxes from the Earth surface interfere with absorption and atmospheric processes on the path towards the sensor (ESA, 2014a). These atmospheric absorption and scattering processes are, according to Guanter et al. (2010), the most critical factors when determining the accuracy of the SIF retrieval. Thus, the use of the atmospheric O₂ bands influence the SIF signal since their absorption features are dependent on spatial and temporal variations of absorption, scattering, illumination and observation geometry. Atmospheric scattering is influenced by the varying aerosol load and consequently affects the path length of radiation, which facilitates the estimation of radiative transfer model parameters. Further, the emitted SIF is re-absorbed by the atmosphere and the vegetation, which in turn influences the SIF signal (Meroni et al., 2009). As reported by Guanter et al. (2010), directional effects in vegetation reflectance can lead to different reflectance responses for incoming diffuse and direct solar irradiance and thus, cause biases in SIF retrieval.

Approximately 1% of the acquired SIF₆₈₀ values from the water stress and approximately 1.5% from the heat stress experiment were negative. These negative SIF₆₈₀ values can be caused by sen-

sensor noise and the assumption of a homogeneous and direct irradiance when retrieving the SIF signal. The assumption of equal irradiance for all plants can lead to over or under estimations of SIF values because it ignores the fact of shaded or fully illuminated plants. Consequently, slight negative SIF values within shaded vegetation and small background influences in regions free of vegetation occurred (Pinto et al., 2016). The reason for sensor noise is the low sensor sensitivity of HyPlant and became not only apparent in negative values but also in high standard deviations of SIF₆₈₀. The noise was higher in SIF₆₈₀ than in SIF₇₆₀ as the measured radiance flux is smaller around the O₂-B band than the O₂-A band (Personal communication with Alexander Damm, 2017).

5.3 Sensitivity of sun-induced chlorophyll fluorescence for environmental stress

5.3.1 Heat stress experiment

When evaluating the results of the heat stress experiment, it has to be considered that according to Yamori et al. (2014), the air temperature of 33.7°C on 2nd July 2015 nearly matched with the optimum temperature for photosynthesis in C₃ plants, whereby it was the optimum temperature for photosynthesis in corn (C₄ plant). Further, it should be noted that the leaf temperature of sun exposed leaves is approximately 5-10°C higher than the air temperature (Feller and Vaseva, 2014) and can lead to stress responses (Flexas et al., 2012).

The results of the C₃ crops revealed decreasing SIF₆₈₀ and SIF₇₆₀ values during the heat wave, which coincide with the findings of Ač et al. (2015), though the findings of the SIF₆₈₀/SIF₇₆₀ ratio were not in agreement as they did not decline notably and consistently. However, the decreasing SIF₆₈₀ and SIF₇₆₀ values of the C₃ crops can be attributed to short-term photosynthetic reduction. A possible cause could be partial stomatal closure as a result of increased air and leaf temperature to avoid transpirational water losses. As a consequence, CO₂ assimilation decreased (Feller and Vaseva, 2014), promoting photo-respiration (Scott, 2008). Furthermore, Rubisco activase might have been reduced because the air temperature on 2nd July was >30°C (Feller and Vaseva, 2014) and thus, enhanced the processes of photorespiration and CET (Flexas et al., 2012).

The findings of the structural and water indices, as well as the NDNI of the C₃ crops confirm the reduction of photosynthetic rate. Leaf and canopy water losses cannot be related to reduced soil water availability since corn showed an increase in water content. As a result, decreased water content in C₃ plants suggests that the plants lost water through transpiration (Aroca, 2012). The nitrogen reduction in C₃ crops is linked to the enzyme nitrate reductase, which is negatively affected by abiotic stressors. As reported by Feller and Vaseva (2014), enzyme activity and thus nitrate assimilation can be reduced by heat. This in turn could lead to a decreased functionality of Rubisco since nitrogen is needed for its activation (Voet et al., 2010). In addition, the reduction of nitrogen within the C₃ plants is in accordance with the results of the structural indices (EVI, NDVI and SR), since a decrease in nitrogen content is related to a decrease in the chlorophyll (Herrmann et al., 2010). According to

Houborg et al. (2015), a relationship between chlorophyll content and carboxylation rate can be found due to the fact that chlorophyll is a substantial part of photosynthesis and responds to changing environmental conditions. Thus, chlorophyll reduction of the C_3 crops during the heat wave correlated with the photosynthetic decrease and confirmed the indication of structural changes.

Changing PRI values during the heat wave can be linked to the conversion of violaxanthin to zeaxanthin within the xanthophyll cycle (Gamon et al., 1997), structural changes, variations in illumination or changes in LAI (Barton and North, 2001). Because the structural indices revealed a decrease in chlorophyll content, the changing PRI values might be related to the xanthophyll cycle since zeaxanthin is linked to NPQ, which prevents the formation of ROS (Murchie and Lawson, 2013). As a result, corn and rapeseed were might have been able to better protect their photosynthetic apparatus than barley and wheat. This finding might also account for the stronger decrease in SIF_{760} values and consequently the slight increase in the SIF ratio of rapeseed (Figure 9b, c and j). The fact that the PRI values of barley, corn and wheat were consistent with the structural indices indicates a decrease in chlorophyll content in barley and wheat and an increase in corn. Yet, this contrasts the findings of the SIF_{680}/SIF_{760} ratio values since they are inversely related to the chlorophyll content (Buschmann, 2007). Nevertheless, the SIF_{680}/SIF_{760} ratio values of rapeseed were consistent with the findings of the structural indices, which revealed a decrease of chlorophyll content in rapeseed. Consequently, the PRI and the SIF_{680}/SIF_{760} ratio values of the heat stress experiment imply not only structural changes but also changes in illumination conditions and LAI since all crops grew during the experiment.

Corn exhibited unlike the C_3 crops, an increase of SIF, chlorophyll, water, nitrogen and xanthophyll pigment content during the heat wave (Figure 9). The combination of these findings suggests that corn was growing and increasing biomass production. Especially since plant growth is directly related to photosynthetic efficiency (Tkemaladze and Makhashvili, 2016) and nitrogen availability enhances biomass production (Cechin, 1998). Moreover, corn exhibited the highest SIFI when compared to the C_3 plants and a different stress response because the majority part of the TSFI values were negative. Consequently, corn showed no heat stress response but indicates a different stress response.

Summarizing the results of the heat stress experiment, the added value of SIF was mainly manifested in the SIFI as the Pearson correlation of all crops exhibited the lowest correlation between SIFI and the VIs. Further, each crop species revealed unique characteristics and sensitivities in their stress responses.

5.3.2 Light stress experiment

The light stress experiment revealed an exponential increase in SIF values with increasing light intensity. This research finding reflects the Kautsky effect as described in Section 2.2.2, which plays a central role in the photosynthesis of sun flecks (Flexas et al., 2012) and is illustrated in Figure 22a. When the findings of the SIF_{680} and SIF_{760} (Figure 22b) were compared with the documented Kaut-

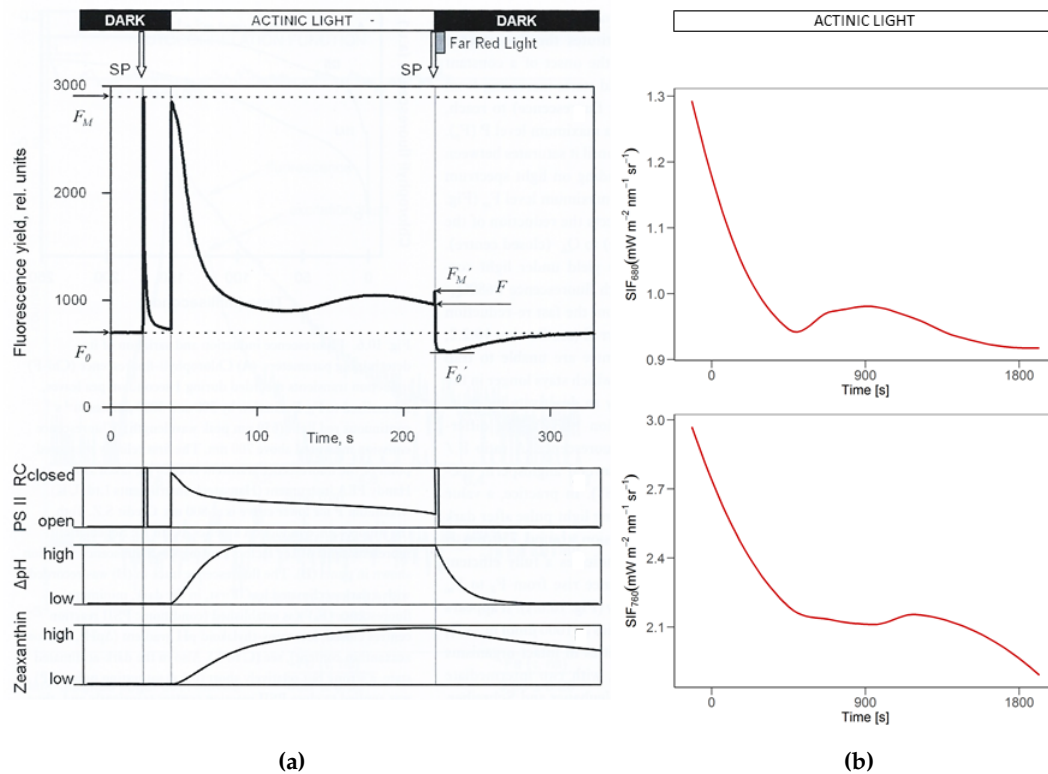


Figure 22: Illustration of the Kautsky effect. The left image (a) was illustrated by Flexas et al. (2012) whereby the right image (b) represents the results of SIF_{680} and SIF_{760} values during the light stress experiment. According to Flexas et al. (2012), F_0 refers to the minimum chlorophyll fluorescence, F'_0 to minimum chlorophyll fluorescence in the light acclimated state, F_M to maximum chlorophyll fluorescence, F'_M to maximum chlorophyll fluorescence under illumination and SP to saturating light pulse.

sky effect from Flexas et al. (2012) it is clearly visible that all fluorescence curves exhibit the same light response. Fluorescence was highest at the time of sudden light exposure and decreased subsequently. The sudden increase in fluorescence occurred because the Q_a acceptor of PSII was reduced at sudden light exposure. As a result, the reaction centres were closed and the incoming photons stayed in the antenna longer, dissipating their energy through fluorescence (Flexas et al., 2012). In addition, the pH gradient and zeaxanthin concentration are inversely related SIF. The increased pH gradient reflects the alkalinisation of the thylakoid lumen due to photosynthetic electron transfer. This increased NPQ and favoured the conversion of violaxanthin to zeaxanthin (Trubitsin et al., 2015). Since SIF_{760} exhibited the same but weakened stress response, it suggests that the reaction centres of PSI were closed as well, leading to higher fluorescence emission as a result of the reduction of the primary acceptor A_0 . Referring to Murchie and Lawson (2013) the subsequent decrease in fluorescence within minutes is termed quenching and occurred during light activation of photosynthesis and stomata opening. As a result, PSII acceptors were re-oxidized and NPQ increased (Trubitsin et al., 2015).

In addition, Kautsky and Hirsch (1931) documented the temperature dependency of fluorescence quenching. They detected that fluorescence revealed a stronger and faster decrease at higher temperatures (30°C) than at lower temperatures (0°C). Consequently, the photosystems adapt faster to actinic light intensities at higher temperatures (Kautsky and Hirsch, 1931) based on the assumption of an optimum temperature range for photosynthesis. Furthermore, Trubitsin et al. (2015) described the influences of illumination pre-conditioning on fluorescence characteristics. Leaves without pre-illumination before adapted to darkness revealed a slower decrease in fluorescence than pre-illuminated leaves. The accelerated decrease of fluorescence in pre-illuminated leaves describes the light-induced NPQ as well as the activation of enzymes (ferredoxin-NADP-reductase and Calvin cycle enzymes). Both, SIF_{680} and SIF_{760} values of the light stress experiment exhibited a fast decrease in SIF (Figure 22b) during the light experiment since it was conducted under high air temperature (>30°C) and with pre-illuminated leaves.

The values of the SIF_{680}/SIF_{760} ratio and the SR revealed a slight tendency of higher chlorophyll content within increased light stress. Approximately 15 minutes before the aircraft passed there was a short second increase of SIF_{680} and SIF_{680}/SIF_{760} values and decrease of SR and LSF values. Interestingly, SIF_{760} exhibited the same short but smaller second increase a few minutes delayed (approximately 5-10 minutes). Though it is mainly visible in the SIF_{680} values it is assumed that this finding was related to PSII. As a result, this finding might illustrate the gradual re-oxidation of the LET. The re-oxidation of LET is accompanied by a short weakening of PSII activity due to the generation of the thylakoid proton gradient and the accelerated electron transport from PSI to the Calvin cycle (Trubitsin et al., 2015).

The characteristic curve of the Kautsky effect was only visible for the SIF_{680} and SIF_{760} values which indicate, in addition to the Pearson correlation coefficients, a high added value of SIF measurements as opposed to VIs. Like the SIF_{680} and SIF_{760} values, the SIFI revealed an exponential increase with increasing light intensity, emphasizing the good performance of the stress index. Furthermore, SIF showed the capability to detect highly dynamic processes and that upscaling of laboratory fluorescence experiments to the field is possible.

5.3.3 Water stress experiment

The results of the water stress experiment showed that drought stressed sugar beet had lower SIF values compared to unstressed sugar beet indicating lower photosynthetic activity. This lower photosynthetic activity can originate from several possible causes.

Short-term responses of lower photosynthetic activity are indicative of stomatal closure and damage of photosynthetic apparatus (Flexas et al., 2012). Both stress responses are not only related to water stress but also to high solar irradiance. This fact became apparent in SIF_{680} and SIF_{760} peaks at solar noon as solar irradiance was highest. According to Kadioglu et al. (2012), stomatal closure is the main plant stress response caused by water stress and was reported by Gamon et al. (1997) in relation to high light intensities at midday. Through the co-occurrence of both water stress and

high light intensities, it is most likely that the sugar beets closed their stomata to limit water losses through transpiration (Willey, 2016). Consequently, the photosynthetic rate decreased due to lowered CO₂ availability (Flexas et al., 2012). Additionally, it could be that damage to the photosynthetic apparatus occurred because the photosystems were not able to use the absorbed light energy (Melis, 1999) at midday. This in turn suggests an enhanced reduction in photosynthetic efficiency (Zhu et al., 2010) and the increase in SIF (Mohammed et al., 2014).

The peculiarity of lower SIF₆₈₀ values at solar noon from unstressed sugar beet compared to stressed sugar beet on field 1 suggests either illumination effects or leaf movement of unstressed sugar beet. Leaves are typically moved in order to avoid direct sunlight exposure, reducing photo-damage and photo-inhibition (Pastenes et al., 2004). Consequently, drought stressed sugar beet on field 1 might not have been able to move its leaves and thus, experienced more photo-damage than water unstressed sugar beet, which could account for higher SIF₆₈₀ values.

In contrast to short-term responses, long-term drought stress responses of sugar beet plants became apparent in early senescence and plant tissue death due to resource reallocation from shoot to root (Gray and Brady, 2016). Senescence and plant tissue death are irreversible damages, which were not only visible in Figure 5 but also reflected by reduced SR and increased SIF₆₈₀/SIF₇₆₀ values of water stressed sugar beet since senescence reduces leaf area and chlorophyll content (Aroca, 2012). Further, the values of SIF₇₆₀ showed, compared to SIF₆₈₀, a stronger decrease between stressed and unstressed sugar beet status. This finding is in accordance with the findings of Ač et al. (2015), who reported a stronger water stress recognisability in the far-red SIF spectrum.

The fluorescence stress indices (SIFI and WSFI) confirmed that unstressed sugar beet was not water stressed since the SIFI values were very low and remained stable during the three measurements. Further, the WSFI averages of unstressed sugar beet were approximately zero. Nevertheless, stressed sugar beet on field 2 revealed, in contrast to stressed sugar beet on field 1, a different behaviour of both SIFI and WSFI during the three measurements. Stressed sugar beet on field 2 showed the lowest SIFI and WSFI values at solar noon, whereby stressed sugar beet on field 1 had lowest SIFI and WSFI values after solar noon. Thus, SIFI and WSFI values of stressed sugar beet on field 2 followed the diurnal course of solar radiation, which implies that lower SIFI and WSFI values might occur due to increased light intensity.

The findings of the water stress experiment represent long-term and short-term stress responses due to the co-occurrence of high light intensities during midday and drought. Again, the SIF₆₈₀, SIF₇₆₀ and SIFI revealed a high added value compared with the SR.

5.4 Monitoring of environmental stress impacts

The localisation of the three stress experiments in the bi-dimensional parameter space confirmed the findings of the previous sections. It is clearly visible that rising stress levels lead to increasing

SIFI and SFI values. The positioning of the water stress experiment was consistent with the water stress results of the meta-analysis by Mohammed et al. (2014). In contrast, the positioning of the heat stress experiment did not coincide with the findings of the meta-analysis. The explanation for this could be that both the C_3 crops and corn influenced the arrangement. The C_3 crops were only slightly heat stressed and corn was not heat stressed. Thus, corn influenced the localisation of the heat stress experiment into opposite direction (Figure 19). Moreover, due to the fact that all crops were growing during the heat stress experiment, biomass increased and might have reduced the C_3 stress response and enhanced the stress response of corn in the opposite direction (Personal meeting with Alexander Damm, 2017). Lastly, light, as an environmental stressor, clearly positioned in the upper part. Since it was the first time that light was implemented in the bi-dimensional parameter space, its positioning has not been confirmed. Nevertheless, the analysis of different stress types in the bi-dimensional parameter space is impeded by overlapping areas (Figure 18) as stress types are not illustrated in isolation but co-occur in the bi-dimensional parameter space, as in a nature. Even when the combination of stressors is known, it is not clear to what proportion the different stressors influence plant responses. A possible solution would be the extension of the dimensions as combined occurrence of stresses could potentially be disentangled (Personal meeting with Alexander Damm, 2017), facilitating stress analysis and stress type determination.

The strongest indicator to monitor environmental stress impacts is the SIFI, as it is directly related to stress intensity and displayed valuable results. Furthermore, the SIFI revealed temporally dynamic variations in plant stress responses and is not restricted to plant species and stress type. Especially the boundlessness of stress type is crucial when interpreting environmental impacts on plant functioning if the stress factors are a priori unknown. This is also the reason why the SFI (LSFI, TSFI, WSFI, etc.) is impeded by its application. Additionally, the application of SFI is inaccurate because it is only a rough estimation to what degree a specific stress influences plant responses. Further, the use of the SIF_{680}/SIF_{760} ratio within this study showed that the SIF ratio did not always provide valuable information on plant stress responses. This might be as the SIF_{680}/SIF_{760} ratio is mainly related to chlorophyll content (Buschmann, 2007). Consequently, structural changes which are not primarily related to plant stress could potentially be misinterpreted.

With reference to the hypothesis SIF can, in contrast to VIs, provide added value for the detection of plant stress responses. This was demonstrated in all three experiments as SIF revealed spatio-temporal patterns which remained undetected with conventional VIs. Moreover, the Pearson correlation between SIF and VIs was low, indicating a high added value of SIF. Therefore, SIF adds value as it is directly related to photosynthetic efficiency and allows for earlier detection of plant stress responses. Moreover, the experiments showed that SIF allows better understanding of actual plant photosynthetic processes when stress type and environmental conditions are known. The combination of SIF and different VIs, as well as the measurement of both SIF_{680} and SIF_{760} signals greatly advanced the understanding of plant functioning. Nevertheless, process understanding of plant functioning under environmental stresses still remain poorly understood as the possible explanations are often based on conjecture.

6 Conclusion

Common and new Earth observation approaches revealed valuable insights into plant functioning under different environmental stress impacts. The application of SIF provided high added value compared to VIs. Especially the light and water stress experiment revealed the potential of SIF to monitor highly dynamic plant stress responses which remained undetected in VIs. Further, both experiments exhibited variations in SIF due to changes in PAR. In contrast, the heat stress experiment revealed that SIF is able to detect distinct stress responses of plant species under equal environmental conditions. Furthermore, the heat and water experiment showed the potential of SIF to detect changes in biomass. It was demonstrated within this master thesis that it is indispensable that VIs with SIF signals are combined to get insights into underlying plant processes since SIF is directly related to photosynthetic efficiency and VIs are related to plant characteristics. The combined application of SIF and VIs showed the potential to detect environmental stress impacts on plant functioning and underlying processes.

Furthermore, the experimental findings underline the combined application of both SIF₆₈₀ and SIF₇₆₀ signals to provide crucial information on plant stress responses. Calculations of fluorescence stress indices like the SIFI are not possible without the simultaneous acquisition of both SIF₆₈₀ and SIF₇₆₀. All experiments illustrated the high potential of SIFI as a strong indicator of plant stress detection. Yet, this finding needs further investigation since it was the first time this stress index was applied to study plant stress responses in terms of solely passive SIF measurements and field experiments.

Nevertheless, this master thesis shows the limitations of the experiments and the methods applied. To emphasize a better consistent comparison between SIF and VIs, all nine VIs of the heat stress experiment must also be considered in the light and water stress experiment. Additionally, the stress experiment was not a stress experiment and for the first time displayed in the bi-dimensional parameter space. I suggest further experiments, which are specifically designed and optimised to represent light stress. The water stress experiment was not designed to monitor process operation of increasing drought stress as it examined the distinct responses of drought stressed and unstressed plants to the daily course of solar irradiation. Thus, I recommend to conduct stress experiments while monitoring how the plant stress responses progress to gain insights to underlying mechanisms. Especially since this plant stress progress will be subject to prospective plant monitoring and assessments in terms of environmental stress impacts on ecosystem functions and yield.

References

- Ač, A., Malenovský, Z., Olejníčková, J., Gallé, A., Rascher, U. and Mohammed, G. (2015). Meta-analysis assessing potential of steady-state chlorophyll fluorescence for remote sensing detection of plant water, temperature and nitrogen stress. *Remote Sensing of Environment*, 168, 420–436.
- Ač, A., Malenovský, Z., Urban, O., Hanuš, J., Zitová, M., Navrátil, M., Vráblová, M., Olejníčková, J., Špunda, V. and Marek, M. (2012). Relation of Chlorophyll Fluorescence Sensitive Reflectance Ratios to Carbon Flux Measurements of Montanne Grassland and Norway Spruce Forest Ecosystems in the Temperate Zone. *The Scientific World Journal*, 2012, 1–13.
- Alberts, B. (2005). *Lehrbuch der Molekularen Zellbiologie*. 3. aufl. edn. Weinheim: WILEY-VCH.
- Ali, M., Montzka, C., Stadler, A., Menz, G., Thonfeld, F. and Vereecken, H. (2015). Estimation and Validation of RapidEye-Based Time-Series of Leaf Area Index for Winter Wheat in the Rur Catchment (Germany). *Remote Sensing*, 7(3), 2808–2831.
- Alonso, L., Gómez-Chova, L., Vila-Francés, J., Amorós-López, J., Guanter, L., Calpe, J. and Moreno, J. L. (2008). Improved Fraunhofer Line Discrimination Method for Vegetation Fluorescence Quantification. *IEEE Geoscience and Remote Sensing Letters*, 5(4), 620–624.
- Alonso, L., Sabater, N., Vicent, J., Cogliati, S., Rossini, M. and Moreno, J. (2014). *Novel Algorithm for the Retrieval of Solar-Induced Fluorescence from Hyperspectral Data Based on Peak Height of Apparent Reflectance at Absorption Features*. Conference: 5th Intl.WS.on Remote Sensing of Vegetation Fluorescence, at CNES, Paris.
- Aroca, R. (2012). *Plant Responses to Drought Stress: From Morphological to Molecular Features*. Heidelberg: Springer.
- Asrar, G., Fuchs, M., Kanemasu, E. T. and Hatfield, J. L. (1984). Estimating absorbed photosynthetic radiation and leaf-area index from spectral reflectance in wheat. *Agronomy Journal*, 76, 300–306.
- Atherton, J., Nichol, C. J. and Porcar-Castell, A. (2016). Using spectral chlorophyll fluorescence and the photochemical reflectance index to predict physiological dynamics. *Remote Sensing of Environment*, 176, 17–30.
- Barton, C. V. M. and North, P. R. J. (2001). Remote sensing of canopy light use efficiency using the photochemical reflectance index: Model and sensitivity analysis. *Remote Sensing of Environment*, 78(3), 264–273.
- Buschmann, C. (2007). Variability and application of the chlorophyll fluorescence emission ratio red/far-red of leaves. *Photosynthesis Research*, 92(2), 261–271.

- Busetto, L., Meroni, M., Crosta, G. F., Guanter, L. and Colombo, R. (2011). SpecCal: Novel software for in-field spectral characterization of high-resolution spectrometers. *Computers & Geosciences*, 37(10), 1685–1691.
- Campbell, N. A., Reece, J. B. and Markl, J. (2006). *Biologie*. 6. überarb. Aufl. edn. München : Pearson Studium.
- Campus Klein-Altendorf (2010). *Campus Klein-Altendorf*. URL: https://www.cka.uni-bonn.de/standort/copy_of_klima (accessed: 10.02.2017)
- Canarache, A., Vintila, I. and Munteanu, I. (2006). *Elsevier's dictionary of soil science : In English (with definitions), French, German and Spanisch*. Amsterdam: Elsevier.
- Carlson, T. N. and Ripley, D. A. (1997). On the relation between NDVI, fractional vegetation cover, and leaf area index. *Remote Sensing of Environment*, 62(3), 241–252.
- Carter, G. A., Theisen, A. F. and Mitchell, R. J. (1990). Chlorophyll fluorescence measured using the Fraunhofer line-depth principle and relationship to photosynthetic rate in the field. *Plant, Cell & Environment*, 13(1), 79–83.
- Cechin, I. (1998). Photosynthesis and Chlorophyll Fluorescence in Two Hybrids of Sorghum under Different Nitrogen and Water Regimes. *Photosynthetica*, 35(2), 233–240.
- Cendrero-Mateo, M. P., Moran, M. S., Papuga, S. A., Thorp, K. R., Alonso, L., Moreno, J., Ponce-Campos, G., Rascher, U. and Wang, G. (2016). Plant chlorophyll fluorescence: Active and passive measurements at canopy and leaf scales with different nitrogen treatments. *Journal of Experimental Botany*, 67(1), 275–286.
- Cogliati, S., Verhoef, W., Kraft, S., Sabater, N., Alonso, L., Vicent, J., Moreno, J., Drusch, M. and Colombo, R. (2015). Retrieval of sun-induced fluorescence using advanced spectral fitting methods. *Remote Sensing of Environment*, 169, 344–357.
- Damm, A. (2016). *Improved iFLD and F680/F760 maps*. SoyFlex Progress meeting, 2016 May 20, via teleconference.
- Damm, A., Elbers, J., Erler, A., Gioli, B., Hamdi, K., Hutjes, R., Kosvancova, M., Meroni, M., Miglietta, F., Moersch, A., Moreno, J., Schickling, A., Sonnenschein, R., Udelhoven, T., Van Der Linden, S., Hostert, P. and Rascher, U. (2010). Remote sensing of sun-induced fluorescence to improve modeling of diurnal courses of gross primary production (GPP). *Global Change Biology*, 16(1), 171–186.
- Damm, A., Erler, A., Hillen, W., Meroni, M., Schaepman, M. E., Verhoef, W. and Rascher, U. (2011). Modeling the impact of spectral sensor configurations on the FLD retrieval accuracy of sun-induced chlorophyll fluorescence. *Remote Sensing of Environment*, 115(8), 1882–1892.

- Damm, A., Guanter, L., Laurent, V. C. E., Schaepman, M. E., Schickling, A. and Rascher, U. (2014). FLD-based retrieval of sun-induced chlorophyll fluorescence from medium spectral resolution airborne spectroscopy data. *Remote Sensing of Environment*, 147, 256–266.
- Damm, A., Guanter, L., Paul-Limoges, E., van der Tol, C., Hueni, A., Buchmann, N., Eugster, W., Ammann, C. and Schaepman, M. E. (2015). Far-red sun-induced chlorophyll fluorescence shows ecosystem-specific relationships to gross primary production: An assessment based on observational and modeling approaches. *Remote Sensing of Environment*, 166, 91–105.
- Edreva, A. (2005). The importance of non-photosynthetic pigments and cinnamic acid derivatives in photoprotection. *Agriculture, Ecosystems & Environment*, 106(2-3), 135–146.
- ESA (2013). Final Report - Technical Assistance for the Deployment of an advanced hyperspectral imaging sensor during HYFLEX. ESA ESTEC RFQ-3-13566/12/NL/LF. Netherlands.
- ESA (2014a). HyPlant Processing Experiment (HYPER) - Algorithms for the retrieval of sun-induced chlorophyll fluorescence and vegetation parameters. ESA Contract No.4000112890/14/NL/FF/gp. Netherlands.
- ESA (2014b). Technical Assistance for the Deployment of an Advanced Hyperspectral Imaging Sensor during HYFLEX. ESA Contract No. 4000107143/12/NL/FF/If. Netherlands.
- ESA (2015a). *New satellite to measure plant health*. URL: http://www.esa.int/Our_Activities/Observing_the_Earth/New_satellite_to_measure_plant_health (accessed: 20.01.2017)
- ESA (2015b). Report for Mission Selection: FLEX, ESA SP-1330/2 (2 volume series). European Space Agency. Noordwijk, Netherlands.
- ESA (2015c). Technical Assistance for the Deployment of an advanced hyperspectral imaging sensor during FLEX-EU. ESA Contract No. 4000107143/NL/FF/if. Netherlands.
- ESA (2016a). Data Acquisition Report - Technical Assistance for the Deployment of an advanced hyperspectral imaging sensor during SoyFLEX. ESA Contract No. 4000107143/NL/FF/if CCN3. Netherlands.
- ESA (2016b). Final Report - Technical Assistance for the Deployment of an advanced hyperspectral imaging sensor during FLEX-EU. ESA Contract No. 4000107143/12/NL/FF/if. Netherlands.
- Feller, U. and Vaseva, I. I. (2014). Extreme climatic events: impacts of drought and high temperature on physiological processes in agronomically important plants. *Frontiers in Environmental Science*, 2(39), 1–17.
- Flexas, J., Carriquí, M., Coopman, R. E., Gago, J., Galmés, J., Martorell, S., Morales, F. and Diaz-Espejo, A. (2014). Stomatal and mesophyll conductances to CO₂ in different plant groups: Un-

- derrated factors for predicting leaf photosynthesis responses to climate change?. *Plant Science*, 226, 41–48.
- Flexas, J., Loreto, F. and Medrano, H. (2012). *Terrestrial Photosynthesis in a Changing Environment: A Molecular, Physiological, and Ecological Approach*. Cambridge: Cambridge University Press.
- Franck, F., Juneau, P. and Popovic, R. (2002). Resolution of the Photosystem I and Photosystem II contributions to chlorophyll fluorescence of intact leaves at room temperature. *Biochimica et Biophysica Acta*, 1556(2), 239–246.
- Frankenberg, C., Fisher, J. B., Worden, J., Badgley, G., Saatchi, S. S., Lee, J.-E., Toon, G. C., Butz, A., Jung, M., Kuze, A. and Yokota, T. (2011). New global observations of the terrestrial carbon cycle from GOSAT: Patterns of plant fluorescence with gross primary productivity. *Geophysical Research Letters*, 38(17), 1–6.
- Gago, J., Douthe, C., Florez-Sarasa, I., Escalona, J. M., Galmes, J., Fernie, A. R., Flexas, J. and Medrano, H. (2014). Opportunities for improving leaf water use efficiency under climate change conditions. *Plant Science*, 226, 108–119.
- Gamon, A. J., Serrano, L. and Surfus, S. J. (1997). The photochemical reflectance index: an optical indicator of photosynthetic radiation use efficiency across species, functional types, and nutrient levels. *Oecologia*, 112(4), 492–501.
- Gao, B.-C. (1996). NDWI - A normalized difference water index for remote sensing of vegetation liquid water from space. *Remote Sensing of Environment*, 58(3), 257–266.
- Grace, J., Nichol, C., Disney, M., Lewis, P., Quaife, T. and Bowyer, P. (2007). Can we measure terrestrial photosynthesis from space directly, using spectral reflectance and fluorescence?. *Global Change Biology*, 13(7), 1484–1497.
- Gray, S. B. and Brady, S. M. (2016). Plant developmental responses to climate change. *Developmental Biology*, 419(1), 64–77.
- Guanter, L., Alonso, L., Gómez-Chova, L., Amorós-López, J., Vila, J. and Moreno, J. (2007). Estimation of solar-induced vegetation fluorescence from space measurements. *Geophysical Research Letters*, 34(8), 1–5.
- Guanter, L., Alonso, L., Gómez-Chova, L., Meroni, M., Preusker, R., Fischer, J. and Moreno, J. (2010). Developments for vegetation fluorescence retrieval from spaceborne high-resolution spectrometry in the O2-A and O2-B absorption bands. *Journal of Geophysical Research: Atmospheres*, 115(D19), 1–16.
- Guanter, L., Frankenberg, C., Dudhia, A., Lewis, P. E., Gómez-Dans, J., Kuze, A., Suto, H. and Grainger, R. G. (2012). Retrieval and global assessment of terrestrial chlorophyll fluorescence from GOSAT space measurements. *Remote Sensing of Environment*, 121, 236–251.

- Hardisky, M. A., Klemas, V. and Smart, R. M. (1983). The Influence of Soil Salinity, Growth Form, and Leaf Moisture on the Spectral Radiance of *Spartina alterniflora* Canopies. *Photogrammetric Engineering and Remote Sensing*, 49(1), 77–83.
- Herrmann, I., Karnieli, A., Bonfil, D. J., Cohen, Y. and Alchanatis, V. (2010). SWIR-based spectral indices for assessing nitrogen content in potato fields. *International Journal of Remote Sensing*, 31(19), 5127–5143.
- Hill, M. J. (2013). Vegetation index suites as indicators of vegetation state in grassland and savanna: An analysis with simulated SENTINEL 2 data for a North American transect. *Remote Sensing of Environment*, 137, 94–111.
- Houborg, R., McCabe, M. F., Cescatti, A. and Gitelson, A. A. (2015). Leaf chlorophyll constraint on model simulated gross primary productivity in agricultural systems. *International Journal of Applied Earth Observation and Geoinformation*, 43, 160–176.
- Huete, A., Didan, K., Miura, T., Rodriguez, E. P., Gao, X. and Ferreira, L. G. (2002). Overview of the radiometric and biophysical performance of the MODIS vegetation indices. *Remote Sensing of Environment*, 83(2), 195–213.
- Hunt, E. R. J. and Rock, B. N. (1989). Detection of changes in leaf water content using near and middle-infrared reflectances. *Remote Sensing of Environment*, 30, 43–54.
- HyPlant (2014). *HyPlant*. URL: <https://twitter.com/hyplant> (accessed: 16.02.2017)
- IPCC (2014). Climate Change 2014: Synthesis Report. Contribution of Working Groups I, II, and III to the Fifth Assessment Report of the Intergovernmental Panel on Climate Change [Core Writing Team, R.K. Pachauri and L.A. Meyer (eds.)]. IPCC, Geneva, Switzerland, 151pp.
- Jiang, Z., Huete, A. R., Didan, K. and Miura, T. (2008). Development of a two-band enhanced vegetation index without a blue band. *Remote Sensing of Environment*, 112(10), 3833–3845.
- Joiner, J., Yoshida, Y., Guanter, L. and Middleton, E. M. (2016). New methods for the retrieval of chlorophyll fluorescence from hyperspectral satellite instruments: simulations and application to GOME-2 and SCIAMACHY. *Atmospheric Measurement Techniques*, 9(8), 3939–3967.
- Kadioglu, A., Terzi, R., Saruhan, N. and Saglam, A. (2012). Current advances in the investigation of leaf rolling caused by biotic and abiotic stress factors. *Plant Science*, 182, 42–48.
- Kautsky, H. and Hirsch, A. (1931). Neue Versuche zur Kohlensäureassimilation. *Die Naturwissenschaften : Organ der Gesellschaft Deutscher Naturforscher und Ärzte, Organ der Hermann von Helmholtz-Gemeinschaft Deutscher Forschungszentren*, 19(48), 964.
- Libbert, E. (1987). *Lehrbuch der Pflanzenphysiologie*. 4. erweiterte neugestaltete aufl. edn. Stuttgart[etc.]: Fischer. New York.

- Lichtenthaler, H. K., Wenzel, O., Buschmann, C. and Gitelson, A. (1998). Plant Stress Detection by Reflectance and Fluorescence. *Annals of the New York Academy of Sciences*, 851(1), 271–285.
- Lillesand, T. M., Kiefer, R. W. and Chipman, J. W. (2008). *Remote sensing and image interpretation*. 6 edn. Wiley. Hoboken.
- Malenovský, Z., Mishra, K. B., Zemek, F., Rascher, U. and Nedbal, L. (2009). Scientific and technical challenges in remote sensing of plant canopy reflectance and fluorescence. *Journal of Experimental Botany*, 60(11), 2987–3004.
- Melis, A. (1999). Photosystem-II damage and repair cycle in chloroplasts: what modulates the rate of photodamage in vivo?. *Trends in Plant Science*, 4(4), 130–135.
- Meroni, M., Rossini, M., Guanter, L., Alonso, L., Rascher, U., Colombo, R. and Moreno, J. (2009). Remote sensing of solar-induced chlorophyll fluorescence: Review of methods and applications. *Remote Sensing of Environment*, 113(10), 2037–2051.
- Mohammed, G. H., Goulas, Y., Magnani, F., Moreno, J., Olejníčková, J., Rascher, U., van der Tol, C., Verhoef, W., Ač, A., Daumard, F., Gallé, A., Malenovský, Z., Pernokis, D., Rivera, J. P., Verrelst, J. and Drusch, M. (2014). 2012 FLEX/ Sentinel-3 Tandem Mission Photosynthesis Study. ESA ESTEC Contract No.4000106396/12/NL/AF. Netherlands.
- Montzka, C., Bogena, H. R., Weihermuller, L., Jonard, F., Bouzinac, C., Kainulainen, J., Balling, J. E., Loew, A., Dall'Amico, J. T., Rouhe, E., Vanderborght, J. and Vereecken, H. (2013). Brightness Temperature and Soil Moisture Validation at Different Scales During the SMOS Validation Campaign in the Rur and Erft Catchments, Germany. *IEEE Transactions on Geoscience and Remote Sensing*, 51(3), 1728–1743.
- Murchie, E. H. and Lawson, T. (2013). Chlorophyll fluorescence analysis: a guide to good practice and understanding some new applications. *Journal of Experimental Botany*, 64(13), 3983–3998.
- Nouri, M.-Z., Moumeni, A. and Komatsu, S. (2015). Abiotic Stresses: Insight into Gene Regulation and Protein Expression in Photosynthetic Pathways of Plants. *International Journal of Molecular Sciences*, 16(9), 20392–20416.
- Panigada, C., Celesti, M., Tagliabue, G., Cogliati, S., Schickling, A., Colombo, R. and Rossini, M. (2016). *Ground fluorescence measurements in SoyFLEX campaign*. SoyFlex Final Meeting, 2016 May 20, via teleconference.
- Panigada, C., Rossini, M., Meroni, M., Cilia, C., Busetto, L., Amaducci, S., Boschetti, M., Cogliati, S., Picchi, V., Pinto, F., Marchesi, A. and Colombo, R. (2014). Fluorescence, PRI and canopy temperature for water stress detection in cereal crops. *International Journal of Applied Earth Observation and Geoinformation*, 30, 167–178.

- Pastenes, C., Porter, V., Baginsky, C., Horton, P. and González, J. (2004). Paraheliotropism can protect water-stressed bean (*Phaseolus vulgaris* L.) plants against photoinhibition. *Journal of Plant Physiology*, 161(12), 1315–1323.
- Peñuelas, J. and Filella, I. (1998). Visible and near-infrared reflectance techniques for diagnosing plant physiological status. *Trends in Plant Science*, 3(4), 151–156.
- Peñuelas, J., Filella, I., Biel, C., Serrano, L. and Savé, R. (1993). The reflectance at the 950-970 nm region as an indicator of plant water status. *International Journal of Remote Sensing*, 14(10), 1887–1905.
- Pinto, F., Damm, A., Schickling, A., Panigada, C., Cogliati, S., Müller-Linow, M., Balvora, A. and Rascher, U. (2016). Sun-induced chlorophyll fluorescence from high-resolution imaging spectroscopy data to quantify spatio-temporal patterns of photosynthetic function in crop canopies. *Plant, Cell & Environment*, 39(7), 1500–1512.
- Plascyk, J. A. (1975). MK II Fraunhofer Line Discriminator (FLD-II) for airborne and orbital remote sensing of solar-stimulated luminescence. *Optical Engineering*, 14(4), 339–346.
- Porcar-Castell, A., Tyystjärvi, E., Atherton, J., van der Tol, C., Flexas, J., Pfündel, E. E., Moreno, J., Frankenberg, C. and Berry, J. A. (2014). Linking chlorophyll a fluorescence to photosynthesis for remote sensing applications: mechanisms and challenges. *Journal of Experimental Botany*, 65(15), 4065–4095.
- Rafferty, J. P. (2015). *Heat wave*. URL: <https://www.britannica.com/science/heat-wave-meteorology> (accessed: 18.03.2017)
- Rascher, U., Agati, G., Alonso, L., Cecchi, G., Champagne, S., Colombo, R., Damm, A., Daumard, F., de Miguel, E., Fernandez, G., Franch, B., Franke, J., Gerbig, C., Gioli, B., Gómez, J. A., Goulas, Y., Guanter, L., Gutiérrez-de-la Cámara, Ó., Hamdi, K., Hostert, P., Jiménez, M., Kosvancova, M., Lognoli, D., Meroni, M., Miglietta, F., Moersch, A., Moreno, J., Moya, I., Neininger, B., Okujeni, A., Ounis, A., Palombi, L., Raimondi, V., Schickling, A., Sobrino, J. A., Stellmes, M., Toci, G., Toscano, P., Udelhoven, T., van der Linden, S. and Zaldei, A. (2009). CEFLES2: the remote sensing component to quantify photosynthetic efficiency from the leaf to the region by measuring sun-induced fluorescence in the oxygen absorption bands. *Biogeosciences*, 6(7), 1181–1198.
- Rascher, U., Alonso, L., Burkart, A., Cilia, C., Cogliati, S., Colombo, R., Damm, A., Drusch, M., Guanter, L., Hanus, J., Hyvärinen, T., Julitta, T., Jussila, J., Kataja, K., Kokkalis, P., Kraft, S., Kraska, T., Matveeva, M., Moreno, J., Muller, O., Panigada, C., Pikel, M., Pinto, F., Prey, L., Pude, R., Rossini, M., Schickling, A., Schurr, U., Schüttemeyer, D., Verrelst, J. and Zemek, F. (2015). Sun-induced fluorescence - a new probe of photosynthesis: First maps from the imaging spectrometer HyPlant. *Global Change Biology*, 21(12), 4673–4684.

- Raven, P. H., Evert, R. F. and Eichhorn, S. E. (2006). *Biologie der Pflanzen*. 4. Aufl. edn. Berlin: De Gruyter.
- Rossini, M., Nedbal, L., Guanter, L., Ač, A., Alonso, L., Burkart, A., Cogliati, S., Colombo, R., Damm, A., Drusch, M., Hanus, J., Janoutova, R., Julitta, T., Kokkalis, P., Moreno, J., Novotny, J., Panigada, C., Pinto, F., Schickling, A., Schüttemeyer, D., Zemek, F. and Rascher, U. (2015). Red and far red Sun-induced chlorophyll fluorescence as a measure of plant photosynthesis. *Geophysical Research Letters*, 42(6), 1632–1639.
- Ruban, A. V. (2015). Evolution under the sun: optimizing light harvesting in photosynthesis. *Journal of Experimental Botany*, 66(1), 7–23.
- Scott, P. (2008). *Physiology and Behaviour of Plants*. Hoboken, N.J: Wiley.
- Serrano, L., Peñuelas, J. and Ustin, S. L. (2002). Remote sensing of nitrogen and lignin in Mediterranean vegetation from AVIRIS data: Decomposing biochemical from structural signals. *Remote Sensing of Environment*, 81(2), 355–364.
- Serrano, L., Ustin, S. L., Roberts, D. A., Gamon, J. A. and Peñuelas, J. (2000). Deriving Water Content of Chaparral Vegetation from AVIRIS Data. *Remote Sensing of Environment*, 74(3), 570–581.
- Sims, D. A. and Gamon, J. A. (2003). Estimation of vegetation water content and photosynthetic tissue area from spectral reflectance: a comparison of indices based on liquid water and chlorophyll absorption features. *Remote Sensing of Environment*, 84(4), 526–537.
- Sztatelman, O., Waloszek, A., Katarzyna Banaś, A. and Gabryś, H. (2010). Photoprotective function of chloroplast avoidance movement: In vivo chlorophyll fluorescence study. *Journal of Plant Physiology*, 167(9), 709–716.
- Tkemaladze, G. and Makhashvili, K. A. (2016). Climate changes and photosynthesis. *Annals of Agrarian Science*, 14(2), 119–126.
- TR32 (2017). *Transregional Collaborative Research Centre 32*. URL: <http://tr32new.uni-koeln.de/index.php/main-menu-entry/why-tr32> (accessed: 06.04.2017)
- Trubitsin, B. V., Vershubskii, A. V., Priklonskii, V. I. and Tikhonov, A. N. (2015). Short-term regulation and alternative pathways of photosynthetic electron transport in *Hibiscus rosa-sinensis* leaves. *Journal of Photochemistry and Photobiology B: Biology*, 152, Part, 400–415.
- Tucker, C. J. (1979). Red and Photographic Infrared Linear Combinations for Monitoring Vegetation. *Remote Sensing of Environment*, 8, 127–150.
- Verhoef, W. and Bach, H. (2003). Simulation of hyperspectral and directional radiance images using coupled biophysical and atmospheric radiative transfer models. *Remote Sensing of Environment*, 87(1), 23–41.

- Vilfan, N., Yang, P., van der Tol, C., Muller, O., Cendrero-Mateo, M. P., Muller-Linow, M. and Rascher, U. (2016). *SoyFLEX WP - 2.6 results*. SoyFlex Progress meeting, 2016 May 20, via tele-conference.
- Voet, D. J., Voet, J. G. and Pratt, C. W. (2010). *Lehrbuch der Biochemie*. 2., aktual. und erw. Aufl. edn. Weinheim: WILEY-VCH.
- Wieneke, S., Ahrends, H., Damm, A., Pinto, F., Stadler, A., Rossini, M. and Rascher, U. (2016). Airborne based spectroscopy of red and far-red sun-induced chlorophyll fluorescence: Implications for improved estimates of gross primary productivity. *Remote Sensing of Environment*, 184, 654–667.
- Willey, N. (2016). *Environmental Plant Physiology*. New York: Garland Science Taylor & Francis.
- Yamori, W., Hikosaka, K. and Way, D. A. (2014). Temperature response of photosynthesis in C3, C4, and CAM plants: temperature acclimation and temperature adaptation. *Photosynthesis Research*, 119(1), 101–117.
- Yang, P., van der Tol, C., Rascher, U., Damm, A., Schickling, A. and Verhoef, W. (in review). Detecting crop functional response to a heat wave using airborne reflectance and sun-induced chlorophyll fluorescence measurements. *Global Change Biology*, .
- Yilmaz, M., Hunt Jr, E. R., Goins, L. D., Ustin, S. L., Vanderbilt, V. C. and Jackson, T. J. (2008). Vegetation water content during SMEX04 from ground data and Landsat 5 Thematic Mapper imagery. *Remote Sensing of Environment*, 112(2), 350–362.
- Yoshida, Y., Joiner, J., Tucker, C., Berry, J., Lee, J.-E., Walker, G., Reichle, R., Koster, R., Lyapustin, A. and Wang, Y. (2015). The 2010 Russian drought impact on satellite measurements of solar-induced chlorophyll fluorescence: Insights from modeling and comparisons with parameters derived from satellite reflectances. *Remote Sensing of Environment*, 166, 163–177.
- Zarco-Tejada, P. J., González-Dugo, V. and Berni, J. A. J. (2012). Fluorescence, temperature and narrow-band indices acquired from a UAV platform for water stress detection using a micro-hyperspectral imager and a thermal camera. *Remote Sensing of Environment*, 117, 322–337.
- Zhu, X.-G., Long, S. P. and Ort, D. R. (2010). Improving Photosynthetic Efficiency for Greater Yield. *Annual Review of Plant Biology*, 61(1), 235–261.
- Zwahr, A. (2006). *Brockhaus Enzyklopädie: In Dreissig Bänden*. Leipzig: F.A. Brockhaus.

Appendix

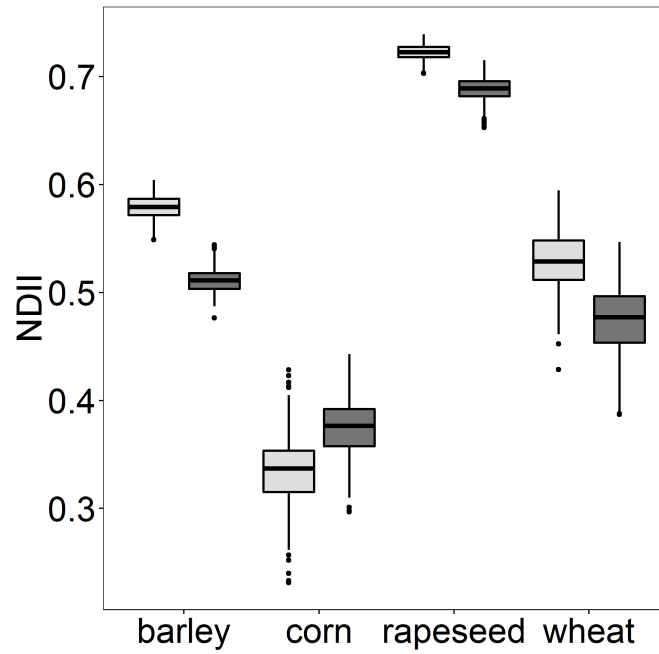


Figure 23: NDII of barley, corn, rapeseed and wheat during the heat wave in summer 2015.